



HAL
open science

Quantum dynamics and geometric phase in $E \otimes e$ Jahn-Teller systems with general C_{nv} symmetry

Thomas Weike, David M. G. Williams, Alexandra Viel, Wolfgang Einfeld

► To cite this version:

Thomas Weike, David M. G. Williams, Alexandra Viel, Wolfgang Einfeld. Quantum dynamics and geometric phase in $E \otimes e$ Jahn-Teller systems with general C_{nv} symmetry. *Journal of Chemical Physics*, 2019, 151 (7), pp.074302. 10.1063/1.5115396 . hal-02267828

HAL Id: hal-02267828

<https://hal.science/hal-02267828>



Submitted on 20 Aug 2019

HAL is a multi-disciplinary open access archive for the deposit and dissemination of scientific research documents, whether they are published or not. The documents may come from teaching and research institutions in France or abroad, or from public or private research centers.

L'archive ouverte pluridisciplinaire **HAL**, est destinée au dépôt et à la diffusion de documents scientifiques de niveau recherche, publiés ou non, émanant des établissements d'enseignement et de recherche français ou étrangers, des laboratoires publics ou privés.

Quantum dynamics and geometric phase in $E \otimes e$ Jahn-Teller systems with general C_{nv} symmetry

Cite as: J. Chem. Phys. **151**, 074302 (2019); <https://doi.org/10.1063/1.5115396>
Submitted: 17 June 2019 . Accepted: 26 July 2019 . Published Online: 19 August 2019

Thomas Weike , David M. G. Williams, Alexandra Viel, and Wolfgang Eisfeld 



View Online



Export Citation



CrossMark

The Journal
of Chemical Physics

Submit Today

The Emerging Investigators Special Collection and Awards
Recognizing the excellent work of early career researchers!



Quantum dynamics and geometric phase in $E \otimes e$ Jahn-Teller systems with general C_{nv} symmetry

Cite as: J. Chem. Phys. 151, 074302 (2019); doi: 10.1063/1.5115396

Submitted: 17 June 2019 • Accepted: 26 July 2019 •

Published Online: 19 August 2019



View Online



Export Citation



CrossMark

Thomas Weike,^{1,a)}  David M. G. Williams,^{1,b)} Alexandra Viel,^{2,c)} and Wolfgang Eisfeld^{1,d)} 

AFFILIATIONS

¹Theoretische Chemie, Universität Bielefeld, Postfach 100131, D-33501 Bielefeld, Germany

²Univ Rennes, CNRS, IPR (Institut de Physique de Rennes) - UMR 6251, F-35000 Rennes, France

^{a)}Electronic mail: t.weike@uni-bielefeld.de

^{b)}Electronic mail: d.williams@uni-bielefeld.de

^{c)}Electronic mail: alexandra.viel@univ-rennes1.fr

^{d)}Electronic mail: wolfgang.eisfeld@uni-bielefeld.de

ABSTRACT

$E \otimes e$ Jahn-Teller (JT) systems are considered the prototype of symmetry-induced conical intersections and of the corresponding geometric phase effect (GPE). For decades, this has been analyzed for the most common case originating from C_{3v} symmetry and these results usually were generalized. In the present work, a thorough analysis of the JT effect, vibronic coupling Hamiltonians, GPE, and the effect on spectroscopic properties is carried out for general C_{nv} symmetric systems (and explicitly for $n = 3-8$). It turns out that the C_{3v} case is much less general than often assumed. The GPE due to the vibronic Hamiltonian depends on the leading coupling term of a diabatic representation of the problem, which is a result of the explicit n , α , and β values of a C_{nv} $E_\alpha \otimes e_\beta$ system. Furthermore, the general existence of n/m ($m \in \mathbb{N}$ depending on n , α , and β) equivalent minima on the lower adiabatic sheet of the potential energy surface (PES) leads to tunneling multiplets of n/m states (state components). These sets can be understood as local vibrations of the atoms around their equilibrium positions within each of the local PES wells symmetrized over all equivalent wells. The local vibrations can be classified as *tangential* or *radial* vibrations, and the quanta in the tangential mode together with the GPE determine the level ordering within each of the vibronic multiplets. Our theoretical predictions derived analytically are tested and supported by numerical model simulations for all possible $E_\alpha \otimes e_\beta$ cases for C_{nv} symmetric systems with $n = 3-8$. The present interpretation allows for a full understanding of the complex JT spectra of real systems, at least for low excitation energies. This also opens a spectroscopic way to show the existence or absence of GPEs.

Published under license by AIP Publishing. <https://doi.org/10.1063/1.5115396>

I. INTRODUCTION

The study of vibronic energy levels supported by doubly degenerate electronic states affected by the Jahn-Teller (JT) effect is a long standing subject studied for more than 60 years.^{1,2} In particular, the degenerate E state of a C_{3v} symmetric system has been the subject of many theoretical investigations. Several authors tackled the problem of the $E \otimes e$ case thoroughly.³⁻⁸ They conclude that due to the presence of the conical intersection and the associated geometric phase effect (GPE), the lowest vibronic state of such a system is doubly degenerate. A broad and thorough discussion of the GPE can be found in the excellent review by Mead⁹ and in the

monograph on conical intersections, edited by Domcke, Yarkony, and Köppel.¹⁰ Despite the widespread assumption that such JT systems generally have a double degenerate vibronic ground state, it has been shown for the $E \otimes e$ case of C_{3v} in a couple of studies that this is only valid up to a certain strength of the quadratic couplings.^{11,12} It was shown that with strong quadratic but weak linear couplings, the vibronic ground state is nondegenerate. In most studies, both a linear coupling term and a quadratic vibronic coupling term are considered, resulting in a lower adiabatic potential surface with three identical local wells. For all strengths of the linear and quadratic vibronic coupling terms, the symmetry induced conical intersection at high symmetry configurations is present

and is located in a region usually relevant for the vibronic ground state wave function. It has been shown by Zwanziger and Grant that three additional conical intersections exist on a circle around the symmetry point and at higher energy.⁶ For particularly strong quadratic but weak linear couplings, these additional conical intersections away from the high symmetry point are driven lower in energy such that they become relevant for the vibronic ground state. These additional conical intersections together with the symmetry induced one are the reason for the nondegenerate vibronic ground state. This is coherent with the widespread “rule” that the symmetry of a vibronic level depends on the number of encircled conical intersections (odd or even).

In real systems, like the prototypical NO₃ studied by us thoroughly,^{13–15} the coupling terms are not limited to the linear and quadratic low orders. Additional conical intersections may occur which complicates the picture further. Our previous investigation of the ²E'' state of NO₃ for which the vibronic level ordering pattern is not obvious, motivates the present study.

The aim of the present paper is to investigate the presence of the GPE, its effect on the vibronic quantum dynamics, and the vibronic level structure in C_{*nv*} symmetric Jahn-Teller systems. This is an extension of previous studies only dealing with C_{3*v*}.^{3–8} The cases varying from *n* = 3 to *n* = 8 are considered explicitly in the present work. A general derivation of coupled potential energy surfaces (PESs) of C_{*nv*} symmetric systems is given. It is similar to the procedure developed by us^{13,16,17} and others^{18–21} for the *n* = 3 case. For each C_{*nv*} case, we analyze the conical intersections and their properties (in terms of the GPE) and show that these properties depend on the lowest order coupling terms. To this end, an analytic proof by asymptotic analysis will be given as well as a numerical visualization of the GPE by plotting the vector fields of the adiabatic wave functions. The consequences of the couplings in terms of spectroscopic signature are discussed. The origin of this analyzed effect is that the E ⊗ *e* JT system for C_{*nv*} causes the lower adiabatic PES sheet to have multiple equivalent wells leading to a multiplet structure of the vibronic levels with as many states within each multiplet as the number of wells. The ordering of the levels in these multiplets is indicative of the GPE as will be shown in the present work and as has been recognized in earlier work.^{5,6,9} This systematic study of C_{*nv*} groups with general *n* also accounts for the existence of different *E* representations. All possible combinations of electronic symmetry E_{*α*} with the symmetry of the coupling coordinate *e*_{*β*} are investigated for the E_{*α*} ⊗ *e*_{*β*} JT effect. Our findings and conclusions are supported both by mathematical analysis and numerical quantum dynamics simulations. It turns out that the conclusions drawn from the C_{3*v*} case are less general than widely assumed.

This paper is organized as follows: Sec. II summarizes the relevant symmetry aspects as well as the derivation of the diabatic models. At this point, the diabatic C_{*nv*} symmetric models for arbitrary E_{*α*} ⊗ *e*_{*β*} are derived. Section III focuses specifically on the geometric phase effect induced by the potential energy surfaces and provides a mathematical proof of the GPE properties of general diabatic Hamiltonians and a visualization of the effect. Section IV addresses the effects on the vibronic quantum dynamics, presenting data relevant for spectroscopic

investigations. An analytic analysis and explanation using a Hückel-like next neighbor model is given for the vibronic level structure, and the findings are verified by numerical test calculations. The main aspects and conclusions of the present work are summarized in Sec. V.

II. SYMMETRY AND DIABATIC MODELS

A. Symmetry considerations

The well-known Jahn-Teller effect is a distortion of the molecular geometry due to vibronic coupling within a set of states belonging to a multidimensional irreducible representation (irrep). The best known example is the distortion of a degenerate *E* state of a C_{3*v*} symmetric system along a degenerate set of *e* coordinates, lowering the equilibrium geometry to only C_s due to E ⊗ *e* vibronic coupling. The existence of two-dimensional *E* representations, and thus the existence of degenerate electronic states and vibrational modes, is a general feature of all non-Abelian point groups with a rotational axis of order *n* ≥ 3. The most common molecular point groups of this type are the C_{*nv*} groups which are used here as a general example for our study. The case *n* = 3 has been used extensively in the past to obtain general insight into the effects of the symmetry on the quantum dynamics. However, we will show that this case is much less general than often assumed.

To this end, a closer look at all *E* representations of C_{*nv*} groups is necessary. Quantum mechanical eigenstates and vibrational normal modes must transform like irreps of the molecular symmetry group due to the Wigner theorem.²² Normal modes are just one special case of symmetry-adapted nuclear coordinates suitable to express potential energy surfaces (PESs). Sets of symmetry coordinates belonging to the same two-dimensional irrep *e*_{*β*}, which we label Q_{*βx*} and Q_{*βy*}, can be rotated freely. This can be utilized to transform the symmetry coordinates such that each of the components becomes an eigenfunction of the C_{*n*} rotation operator, the most critical operator of a C_{*nv*} symmetry group. While Q_{*βx*} and Q_{*βy*} are mixed by C_{*n*}, the complex coordinates

$$Q_{\beta\pm} = \frac{1}{\sqrt{2}}(Q_{\beta x} \pm iQ_{\beta y}) = re^{\pm i\beta\phi} \quad (1)$$

are eigenfunctions with respect to C_{*n*} with eigenvalues of $\exp\left(\pm \frac{2i\beta\pi}{n}\right)$. The β in Eq. (1) refers to the kind of the *E* irrep, namely, E_{*β*}. The groups C_{3*v*} and C_{4*v*} only have one *E* irrep, and thus β = 1 is usually omitted, but in general, C_{*nv*} groups have β_{max} irreps E_{*β*} of dimension 2 with

$$\beta_{\max} = \frac{n + n \bmod 2}{2} - 1. \quad (2)$$

For example, C_{5*v*} and C_{6*v*} have two different irreps E₁ and E₂.

The same kind of transformation as for the coordinates Eq. (1) can be applied to the electronic state components of a degenerate electronic state transforming as E_{*α*}, namely,

$$|\psi_{\alpha\pm}\rangle = \frac{1}{\sqrt{2}}(|\psi_{\alpha x}\rangle \pm i|\psi_{\alpha y}\rangle). \quad (3)$$

These are eigenfunctions with respect to \widehat{C}_n with eigenvalues of $\exp(\mp \frac{2i\alpha\pi}{n})$. As has been used in our previous work,¹⁶ both the complex symmetry adapted coordinates and the complex electronic state components are relevant for the derivation of the diabatic models because of their advantageous properties with respect to the rotation operator \widehat{C}_n .

B. General quantum dynamics aspects

The fundamental aspects of the quantum dynamics in any $E_\alpha \otimes e_\beta$ JT system generally can be studied in the two-dimensional subspace of the two e_β nuclear coordinates. It is of advantage to transform the Hamiltonian to polar coordinates which then reads

$$\widehat{H}(r, \phi) = -\frac{1}{2} \left(\frac{\partial^2}{\partial r^2} + \frac{1}{r} \frac{\partial}{\partial r} + \frac{1}{r^2} \frac{\partial^2}{\partial \phi^2} \right) + \mathbf{D}(r, \phi), \quad (4)$$

where $\mathbf{D}(r, \phi)$ is the diabatic PES matrix. The coupling between electronic and nuclear motions is described by the off-diagonal elements of the potential matrix \mathbf{D} , which represents the electronic Hamiltonian in a diabatic electronic state basis. \mathbf{D} may be split into an average potential for both state components, $V\mathbf{1}$, and a coupling matrix V_c . The function V and the matrix V_c can be expanded in series, and the general form of the coupling matrix reads

$$V_c(r, \phi) = \sum_{k=0}^{\infty} \sum_{l=-\infty}^{\infty} c_{kl} r^k \begin{pmatrix} 0 & \exp(il\phi) \\ \exp(-il\phi) & 0 \end{pmatrix}. \quad (5)$$

Note that l can be negative. The coefficients c_{kl} depend on the details of the system, especially symmetry can lead to many vanishing coefficients.

It is of advantage to define l -dependent vibronic angular momentum operators

$$\widehat{J}_l = -i \frac{\partial}{\partial \phi} \begin{pmatrix} 1 & 0 \\ 0 & 1 \end{pmatrix} - \frac{l}{2} \begin{pmatrix} 1 & 0 \\ 0 & -1 \end{pmatrix}, \quad (6)$$

which commute with the term of the Fourier expansion in Eq. (5) having the same l value. This operator will not commute with any other expansion term of V_c having a different l value. In the particular case of a V_c limited to a single l expansion term, \widehat{J}_l presents some interesting properties detailed below. In that case, \widehat{J}_l and V_c can be diagonalized simultaneously. The two eigenfunctions of \widehat{J}_l corresponding to the degenerate eigenvalue $\lambda/2$ are given by

$$\frac{1}{\sqrt{2}} \begin{pmatrix} \exp(i\frac{\lambda+l}{2}\phi) \\ \exp(i\frac{\lambda-l}{2}\phi) \end{pmatrix}, \quad \frac{1}{\sqrt{2}} \begin{pmatrix} \exp(i\frac{\lambda+l}{2}\phi) \\ -\exp(i\frac{\lambda-l}{2}\phi) \end{pmatrix}. \quad (7)$$

It can be shown that λ must be an integer of the same parity as l because of the general properties of angular momentum operators and the requirement that the total wave function must be single-valued. The eigenvectors of \widehat{J}_l are also eigenvectors of the Fourier terms of V_c having the same l value with eigenvalues

$$\Lambda = \pm \sum_{k=0}^{\infty} c_{kl} r^k. \quad (8)$$

This equation also shows that any coupling matrix with a coupling element restricted to a single l value will have cylindrical symmetry

($C_{\infty v}$). Equation (7) can be analyzed with respect to rotation of ϕ by 2π and for $\lambda = 0$, this refers to the purely electronic contribution to the wave function and thus to the electronic angular momentum. For odd l , the electronic contribution to the eigenfunctions changes sign and this implies a nontrivial geometric phase of the nuclear part of the wave function to compensate. This is not the case for even l values. These two cases we will refer to as *fermionic* (odd l) and *bosonic* (even l) behavior, respectively.

C. General derivation of diabatic models

We consider a diabatic $E \otimes e$ model for any system of C_{nv} symmetry, where the highest n -fold rotational axis is denoted by C_n . The general symmetry properties of such systems have been presented in Sec. II A. With the previously defined coordinates and states, a general $E_\alpha \otimes e_\beta$ diabatic model can be constructed by expanding the electronic Hamiltonian in the diabatic state basis as

$$\begin{aligned} \widehat{H} &= \sum_{j,k \in \{+,-\}} |\psi_{\alpha j}\rangle \langle \psi_{\alpha j} | \widehat{H} | \psi_{\alpha k}\rangle \langle \psi_{\alpha k} | \\ &= \sum_{j,k \in \{+,-\}} |\psi_{\alpha j}\rangle D_{jk}^\alpha(Q_{\beta+}, Q_{\beta-}) \langle \psi_{\alpha k} |. \end{aligned} \quad (9)$$

The diabatic PES matrix elements can be expanded to arbitrary order as

$$D_{jk}^\alpha(Q_{\beta+}, Q_{\beta-}) = \sum_{\substack{p,q \\ p+q=m}} \frac{1}{m!} c_{jkpq}^\alpha Q_{\beta+}^p Q_{\beta-}^q, \quad (10)$$

and the invariance condition under symmetry transformations allows us to determine the nonvanishing c_{jkpq}^α terms.

In particular, the invariance when considering the \widehat{C}_n rotational transformation

$$\begin{aligned} |\psi_{\alpha\pm}\rangle (Q_{\beta+})^p (Q_{\beta-})^q \langle \psi_{\alpha\pm} | \\ &= |\widehat{C}_n \psi_{\alpha\pm}\rangle (\widehat{C}_n Q_{\beta+})^p (\widehat{C}_n Q_{\beta-})^q \langle \widehat{C}_n \psi_{\alpha\pm} | \\ &= e^{2i\pi \frac{\beta(p-q)}{n}} |\psi_{\alpha\pm}\rangle (Q_{\beta+})^p (Q_{\beta-})^q \langle \psi_{\alpha\pm} |, \end{aligned} \quad (11a)$$

$$\begin{aligned} |\psi_{\alpha+}\rangle (Q_{\beta+})^p (Q_{\beta-})^q \langle \psi_{\alpha-} | \\ &= |\widehat{C}_n \psi_{\alpha+}\rangle (\widehat{C}_n Q_{\beta+})^p (\widehat{C}_n Q_{\beta-})^q \langle \widehat{C}_n \psi_{\alpha-} | \\ &= e^{2i\pi \frac{\beta(p-q)-2\alpha}{n}} |\psi_{\alpha+}\rangle (Q_{\beta+})^p (Q_{\beta-})^q \langle \psi_{\alpha-} | \end{aligned} \quad (11b)$$

implies conditions on both the diagonal and off-diagonal matrix elements. For the diagonal elements of the diabatic matrix, denoted as $V_n(Q_{\beta+}, Q_{\beta-})$, the resulting condition

$$[\beta(p-q)] \bmod n = 0 \quad (12)$$

is independent of α . By contrast, the condition for nonvanishing off-diagonal elements, denoted by $P_{n\alpha}(Q_{\beta+}, Q_{\beta-})$,

$$[\beta(p-q) - 2\alpha] \bmod n = 0 \quad (13)$$

depends on both α and β . The diabatic matrix potential for $E_\alpha \otimes e_\beta$ is thus

$$D_{n\alpha}(Q_{\beta+}, Q_{\beta-}) = V_n(Q_{\beta+}, Q_{\beta-}) \mathbf{1} + \begin{pmatrix} 0 & P_{n\alpha}(Q_{\beta+}, Q_{\beta-}) \\ P_{n\alpha}^*(Q_{\beta+}, Q_{\beta-}) & 0 \end{pmatrix}. \quad (14)$$

One finds that $V_n(Q_{\beta+}, Q_{\beta-})$ is a totally symmetric offset which does not contribute to the coupling.

A more detailed analysis can be performed on the individual terms of the $P_{n\alpha}(Q_{\beta+}, Q_{\beta-})$ functions. In the expansion of $P_{n\alpha}$, one can first factorize out totally symmetric factors $(Q_{\beta+} Q_{\beta-})^j$ which do not change the symmetry properties as evidenced from a closer look at Eq. (13). This yields

$$P_{n\alpha}(Q_{\beta+}, Q_{\beta-}) = \sum_{p,q} c_{pq}^{n\alpha} Q_{\beta+}^p Q_{\beta-}^q = \sum_{p,q} c_{pq}^{n\alpha} (Q_{\beta+} Q_{\beta-})^j Q_{\beta+}^{p-j} Q_{\beta-}^{q-j}. \quad (15)$$

For each term of the double sum, j can always be chosen to equal either p or q , respectively, $p = q$ being excluded by the constants given in Eq. (13). This allows us to rewrite Eq. (15) as

$$P_{n\alpha}(Q_{\beta+}, Q_{\beta-}) = \sum_{q=0}^{\infty} \sum_{p=q+1}^{\infty} c_{pq}^{n\alpha} (Q_{\beta+} Q_{\beta-})^q Q_{\beta+}^{p-q} + \sum_{p=0}^{\infty} \sum_{q=p+1}^{\infty} c_{pq}^{n\alpha} (Q_{\beta+} Q_{\beta-})^p Q_{\beta-}^{q-p} \quad (16a)$$

TABLE I. Lowest monomials of $P_{n\alpha}(Q_{\beta+}, Q_{\beta-})$ for $E_\alpha \otimes e_\beta$ coupling potential of a C_{nv} system. The ‘‘GPE’’ indicates the presence/absence of a nontrivial geometric phase effect in the ‘‘inner region’’ ($\lambda = 0$) (see text).

n	α	β	Monomials				GPE	Radius of ‘‘inner region’’
3	1	1	Q_-	Q_+^2	Q_-^4	Q_+^5	Yes	$f_{-1}^{31}(0) - f_{+2}^{31}(0) r = 0$
4	1	1	Q_+^2	Q_-^2	Q_+^6	Q_-^6	No	
5	1	1	Q_{1+}^2	Q_{1-}^3	Q_{1+}^7	Q_{1-}^8	No	$f_{+2}^{51}(0) - f_{-3}^{51}(0) r = 0$
	1	2	Q_{2+}	Q_{2-}^4	Q_{2+}^6	Q_{2-}^9	Yes	$f_{+1}^{51}(0) + f_{+1}^{51'}(0) r^2 - f_{-4}^{51}(0) r^3 = 0$
	2	1	Q_{1-}	Q_{1+}^4	Q_{1-}^6	Q_{1+}^9	Yes	$f_{-1}^{52}(0) + f_{-1}^{52'}(0) r^2 - f_{+4}^{52}(0) r^3 = 0$
	2	2	Q_{2+}^2	Q_{2-}^3	Q_{2+}^7	Q_{2-}^8	No	$f_{+2}^{52}(0) - f_{-3}^{52}(0) r = 0$
6	1	1	Q_{1+}^2	Q_{1-}^4	Q_{1+}^8	Q_{1-}^{10}	No	
	1	2	Q_{2+}	Q_{2-}^2	Q_{2+}^4	Q_{2-}^5	Yes	
	2	1	Q_{1-}	Q_{1+}^4	Q_{1-}^8	Q_{1+}^{10}	No	
	2	2	Q_{2-}	Q_{2+}^4	Q_{2-}^4	Q_{2+}^5	Yes	
7	1	1	Q_{1+}^2	Q_{1-}^5	Q_{1+}^9	Q_{1-}^{12}	No	$f_{+2}^{71}(0) + f_{+2}^{71'}(0) r^2 - f_{-5}^{71}(0) r^3 = 0$
	1	2	Q_{2+}	Q_{2-}^6	Q_{2+}^8	Q_{2-}^{13}	Yes	$f_{+1}^{71}(0) + f_{+1}^{71'}(0) r^2 + f_{+1}^{71''}(0) r^4 - f_{-6}^{71}(0) r^5 = 0$
	1	3	Q_{3+}^3	Q_{3-}^4	Q_{3+}^{10}	Q_{3-}^{11}	Yes	$f_{+3}^{71}(0) - f_{-4}^{71}(0) r = 0$
	2	1	Q_{1-}	Q_{1+}^4	Q_{1-}^{10}	Q_{1+}^{11}	Yes	$f_{-2}^{72}(0) - f_{+3}^{72}(0) r = 0$
	2	2	Q_{2+}^2	Q_{2-}^5	Q_{2+}^9	Q_{2-}^{12}	No	$f_{-2}^{72}(0) + f_{+2}^{72'}(0) r^2 - f_{-5}^{72}(0) r^3 = 0$
	2	3	Q_{3-}	Q_{3+}^6	Q_{3-}^8	Q_{3+}^{13}	Yes	$f_{-1}^{72}(0) + f_{-1}^{72'}(0) r^2 + f_{-1}^{72''}(0) r^4 - f_{+6}^{72}(0) r^5 = 0$
	3	1	Q_{1-}	Q_{1+}^6	Q_{1-}^8	Q_{1+}^{13}	Yes	$f_{-1}^{73}(0) + f_{-1}^{73'}(0) r^2 + f_{-1}^{73''}(0) r^4 - f_{+6}^{73}(0) r^5 = 0$
	3	2	Q_{2+}^3	Q_{2-}^4	Q_{2+}^{10}	Q_{2-}^{11}	Yes	$f_{+3}^{73}(0) - f_{-4}^{73}(0) r = 0$
	3	3	Q_{3+}^2	Q_{3-}^5	Q_{3+}^9	Q_{3-}^{12}	No	$f_{+2}^{73}(0) + f_{+2}^{73'}(0) r^2 - f_{-5}^{73}(0) r^3 = 0$
8	1	1	Q_{1+}^2	Q_{1-}^6	Q_{1+}^{10}	Q_{1-}^{14}	No	
	1	2	Q_{2+}	Q_{2-}^3	Q_{2+}^5	Q_{2-}^7	Yes	
	1	3	Q_{3-}	Q_{3+}^6	Q_{3-}^{10}	Q_{3+}^{14}	No	
	2	1	Q_{1+}^4	Q_{1-}^4	Q_{1+}^{12}	Q_{1-}^{12}	No	
	2	2	Q_{2+}^2	Q_{2-}^2	Q_{2+}^6	Q_{2-}^6	No	
	2	3	Q_{3+}^4	Q_{3-}^4	Q_{3+}^{12}	Q_{3-}^{12}	No	
	3	1	Q_{1-}	Q_{1+}^5	Q_{1-}^{10}	Q_{1+}^{14}	No	
	3	2	Q_{2-}	Q_{2+}^3	Q_{2-}^5	Q_{2+}^7	Yes	
	3	3	Q_{3+}^2	Q_{3-}^6	Q_{3+}^{10}	Q_{3-}^{14}	No	

$$= \sum_{k=1}^{\infty} Q_{\beta+}^k \underbrace{\sum_{q=0}^{\infty} c_{(q+k)q}^{n\alpha} (Q_{\beta+} Q_{\beta-})^q}_{f_{+k}^{n\alpha}(Q_{\beta+}, Q_{\beta-})} + \sum_{k=1}^{\infty} Q_{\beta-}^k \underbrace{\sum_{p=0}^{\infty} c_{p(p+k)}^{n\alpha} (Q_{\beta+} Q_{\beta-})^p}_{f_{-k}^{n\alpha}(Q_{\beta+}, Q_{\beta-})} \quad (16b)$$

$$= \sum_{k=1}^{\infty} (f_{+k}^{n\alpha}(Q_{\beta+}, Q_{\beta-}) Q_{\beta+}^k + f_{-k}^{n\alpha}(Q_{\beta+}, Q_{\beta-}) Q_{\beta-}^k). \quad (16c)$$

The $Q_{\beta+}^k$ and $Q_{\beta-}^k$ terms of Eq. (16b) are referred to as monomials in the following. The characteristic properties of the potential considered in the present work do only depend on these monomials but not on the totally symmetric prefactors. For all C_{nv} groups with $n = 3, \dots, 8$ and all combinations of E_{α} and e_{β} , the four lowest orders of such monomials are given in Table I. If higher orders are desired, they can be derived easily following the above general rules. Higher orders beyond the typically used lowest two orders are mainly of interest to improve the quality of PES models for explicit systems (like NO_3 studied by us) in regions farther away from the coordinate origin. They do not change the basic properties of the PES but allow us to treat large amplitude motions of the nuclei more accurately. Equation (16c) gives the expansion in the complex representation of the coordinates $Q_{\beta+}$ and $Q_{\beta-}$ in which $\phi_{\beta} = \beta \cdot \phi$. It is convenient to contract the totally symmetric parts in the expression (16c) resulting in

$$P_{n\alpha}(r_{\beta}, \phi_{\beta}) = \sum_k \left[F_{+k}^{n\alpha}(r_{\beta}) e^{ik\phi_{\beta}} + F_{-k}^{n\alpha}(r_{\beta}) e^{-ik\phi_{\beta}} \right]. \quad (17)$$

For practical applications, the functions $F_{\pm k}^{n\alpha}(r_{\beta})$ can be modeled by any totally symmetric and continuous function of r_{β} . The power expansion of the functions $F_{\pm k}^{n\alpha}(r_{\beta})$ will render Eqs. (15) and (17) equivalent. This form is particularly convenient for the analytic investigation of the properties of the diabatic Hamiltonians as will be seen below.

For the numerical models of $C_{nv} E_{\alpha} \times e_{\beta}$ systems studied here, we limit the expansion of $P_{n\alpha}(Q_{\beta+}, Q_{\beta-})$ to the first two monomials, as given in Table I. The use of at least two monomials is crucial in order to obtain PESs with the symmetry induced multiple equivalent potential wells on the lower adiabat as is characteristic for such Jahn-Teller systems. The order of the expansion used for the diagonal average potential $V_n(Q_{\beta+}, Q_{\beta-})$ is chosen such that the resulting adiabatic potential surfaces are bound. Table I also provides the next two higher monomials for the expansion. In addition, the table provides the information about the presence (or absence) of a geometric phase effect (GPE) as deduced from Eq. (7) for $\lambda = 0$ and each n, α, β . The last column in Table I presents formulas to determine the radius at which the additional conical intersections appear and may change the behavior of the system. This is discussed in detail in Sec. III.

The limitation to the first two coupling monomials in the following is entirely due to practical reasons for the analytical and numerical analysis. Adding higher order terms is only needed to improve the PES accuracy for a real system and

will not (or rather is not supposed to) change the fundamental physics. It should also be kept in mind that adding more and more higher order terms in a Taylor expansion might lead to numerical problems and unphysical behavior. For this reason, a new strategy has been developed by us recently, which is based entirely on the lowest coupling orders and artificial neural networks.²³

III. GEOMETRIC PHASE

The knowledge of the general and generic diabatic models for C_{nv} systems now allows us to analyze their properties. One of the most important and widely discussed properties is the geometric phase effect, an effect usually considered to be induced by the existence of a conical intersection. The nontrivial geometric phase in vibronic coupling systems is just a special case of a Berry phase.²⁴ It is often assumed that the “ $E \otimes e$ ” JT coupling generally induces such a conical intersection and thus the geometric phase effect. However, it will be shown in the following that the existence of a geometric phase effect depends on the type of the $E \otimes e$ system, namely, on n, α , and β .

For most of the systems with the above given diabatic models, the coordinate region of interest usually is what we refer to as the “inner region” where the JT coupling induces multiple equivalent potential wells on the lower adiabatic PES. In most cases, the number of equivalent wells is equal to the order n of the principal C_n axis. For $n \geq 6$, there are also cases with only n/m equivalent minima due to the symmetry properties of the e_{β} coordinates (see Sec. IV). For cases dominated by the inner region, it is relevant to look more closely at the PES for short distances from the symmetry point. Therefore, an asymptotic expansion and analysis in the vicinity of the symmetry point ($r \rightarrow 0$) is performed to investigate the effect of the intersection. The totally symmetric part of the potential can be omitted for the following discussion and will not be considered in this derivation.

In the following, we will illustrate the effects of a geometric phase using the above described generic diabatic models in more detail. It is convenient to transform back the electronic component basis to the real space, namely, $\{|\psi_{\alpha x}\rangle, |\psi_{\alpha y}\rangle\}$, in order to represent the effects graphically. To this end, the eigenvectors of the diabatic PES matrix are determined by solving the following equation:

$$\begin{pmatrix} W^{\alpha}(Q_{\beta+}, Q_{\beta-}) - \Lambda & Z^{\alpha}(Q_{\beta+}, Q_{\beta-}) \\ Z^{\alpha}(Q_{\beta+}, Q_{\beta-}) & -W^{\alpha}(Q_{\beta+}, Q_{\beta-}) - \Lambda \end{pmatrix} \mathbf{c}^{\alpha} = \mathbf{0}, \quad (18)$$

where $W^{\alpha}(Q_{\beta+}, Q_{\beta-}) = \text{Re}(P_{n\alpha}(Q_{\beta+}, Q_{\beta-}))$ and $Z^{\alpha}(Q_{\beta+}, Q_{\beta-}) = \text{Im}(P_{n\alpha}(Q_{\beta+}, Q_{\beta-}))$. The n dependence of W and Z has been dropped for better readability. The resulting eigenvectors of this equation can be expressed in the form

$$\mathbf{c}_{\pm}^{\alpha}(Q_{\beta+}, Q_{\beta-}) = \frac{1}{\sqrt{2(1 \mp W^{\alpha}(Q_{\beta+}, Q_{\beta-}))}} \begin{pmatrix} \pm 1 - W^{\alpha}(Q_{\beta+}, Q_{\beta-}) \\ Z^{\alpha}(Q_{\beta+}, Q_{\beta-}) \end{pmatrix} \quad (19)$$

corresponding to the eigenvalues

$$\Lambda = \pm \sqrt{[W^{\alpha}(Q_{\beta+}, Q_{\beta-})]^2 + [Z^{\alpha}(Q_{\beta+}, Q_{\beta-})]^2}. \quad (20)$$

A relevant quantity to plot in order to visualize the role of the orders l in the coupling part $P_{n\alpha}$ is the vector field of the real valued eigenvectors in the plane of the real coordinates $Q_{\beta x}$ and $Q_{\beta y}$. Figure 1 presents the obtained vector fields for a selection of point groups with single principal axis C_n of order $n = 3, 5, 7$ for α, β combinations featuring a leading coupling term of odd order. As already stated, the numerical model systems are limited to the first two leading monomials in the expansion Eq. (17), as listed in Table I.

Figures 1(a)–1(c) present the vector field in the region of low energy around the origin where n equivalent minima on the lower adiabatic PES sheet are located. The characteristic feature of all of these plots is the existence of one or more slits where the vectors change orientation (“sign”) abruptly. These slits are marked clearly by red lines for the convenience of the reader. The case $n = 3$ is the well-known standard case studied for decades. It clearly shows one slit starting from the origin, confirming the established existence of

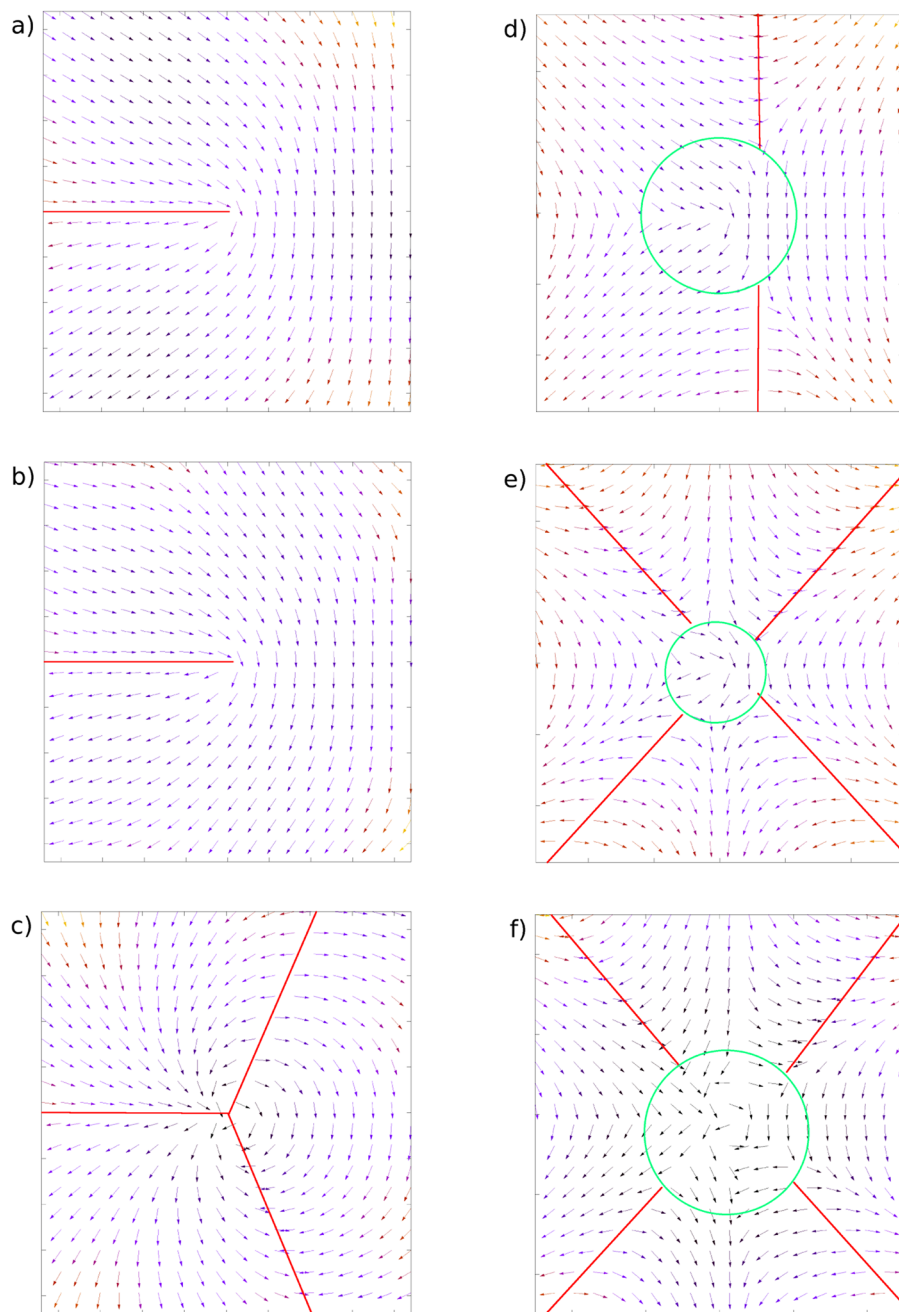


FIG. 1. Vector fields of the eigenvectors corresponding to the lower adiabatic PES plotted in the plane of the $Q_{\beta x}$ and $Q_{\beta y}$ coordinates. (a)–(c) show the inner region for C_{3v} , C_{5v} ($E_1 \otimes e_2$), and C_{7v} ($E_1 \otimes e_3$), respectively. (d)–(f) present the outer region for the same three cases. The green circles indicate the radius separating inner from outer regions.

a geometric phase. The same kind of behavior is found for the case of $n = 5$ for $E_1 \otimes e_2$ ($E_2 \otimes e_1$). Finally, the case $E_1 \otimes e_3$ for $n = 7$ is presented because this is a case in which three slits and a corresponding geometric phase are observed. By contrast, two slits are found for $n = 4$ and C_{5v} ($E_1 \otimes e_1$ or $E_2 \otimes e_2$), respectively, with the consequence that there is no geometric phase in these cases. The corresponding vector fields are presented in Fig. 2. It turns out that the number of slits observed near the origin in the real representation is always equal to the power of the lowest coupling term as is shown below.

To this end, the real valued eigenvectors are analyzed for the limit of small distances from the origin (high symmetry point). In this asymptotic analysis, only the term of the lowest order remains relevant in the expansion of the coupling matrix and therefore the eigenvectors corresponding to the eigenvalues

$$\Lambda = \pm r^k \quad (21)$$

read

$$\mathbf{c}_\pm(\phi) = \frac{1}{\sqrt{2(1 \mp \cos(m\phi))}} \begin{pmatrix} \pm 1 - \cos(m\phi) \\ \sin(m\phi) \end{pmatrix}, \quad (22)$$

where

$$m = \beta k. \quad (23)$$

In the following, only the eigenvector \mathbf{c}_- is considered, but the treatment of \mathbf{c}_+ is completely equivalent. We note that the normalization factor becomes singular for $m\phi = 2\pi j + \pi$, $j = 0, 1, \dots, m - 1$. The behavior of the eigenvectors in the vicinity of these singularities is determined by the limit

$$\lim_{\epsilon \rightarrow 0} \mathbf{c}_- \left(\frac{2\pi j + \pi}{m} \pm \epsilon \right) = \lim_{\epsilon \rightarrow 0} \frac{1}{\sqrt{2(1 + \cos(2\pi j + \pi \pm m\epsilon))}} \times \begin{pmatrix} -1 - \cos(2\pi j + \pi \pm m\epsilon) \\ \sin(2\pi j + \pi \pm m\epsilon) \end{pmatrix}. \quad (24)$$

This limit is evaluated by a Taylor expansion up to first order in the denominator and in the numerator, which yields

$$\begin{aligned} \lim_{\epsilon \rightarrow 0} \mathbf{c}_- \left(\frac{2\pi j + \pi}{m} \pm \epsilon \right) &= \lim_{\epsilon \rightarrow 0} \frac{1}{\sqrt{2} m^2 \epsilon^2} \begin{pmatrix} 0 \\ \pm m\epsilon \end{pmatrix} \\ &= \lim_{\epsilon \rightarrow 0} \pm \frac{1}{\sqrt{2}} \begin{pmatrix} 0 \\ 1 \end{pmatrix}. \end{aligned} \quad (25)$$

This implies a discontinuity for each angle $\phi = (2\pi j + \pi)/m$, and thus a total of m slits, with m being the order of the coupling term.

While this explains the behavior of the vector fields shown in Figs. 1 and 2 for small distances r from the origin, it fails to describe the $r \gg 1$ outer region. Figures 1(d)–1(f) and 2(b) show the same five systems considered before but now with focus on the region for larger radius $r \gg 1$ and thus for higher energies. The radius at which the additional conical intersections occur is indicated by green circles in Figs. 1 and 2. The $n = 3$ case obviously has two slits starting at this radius whereas the slit starting from the origin vanishes. By contrast, no change is seen for $n = 4$ and the $E_1 \otimes e_1$ ($E_2 \otimes e_2$) case of $n = 5$. The two remaining cases, $n = 5$ $E_1 \otimes e_2$ ($E_2 \otimes e_1$) and $n = 7$ $E_1 \otimes e_3$, result in 4 slits in the outer region. The explanation of this behavior can be gained from a closer look at the two adiabatic PES sheets for these systems. We present two views of the adiabatic PESs plotted in the two-dimensional space of Q_x and Q_y for $n = 3$ in Fig. 3. It becomes apparent from Fig. 3(a) that the PESs fulfill the 3-fold symmetry and invariance properties as required and enforced by construction of the model. In Fig. 3(b), the representation of the bound PESs is restricted to $Q_x > 0$. The well-known conical intersection is seen at the origin and marked by a green circle. An additional conical intersection is clearly visible for larger r and higher energy, also marked by a green circle. Due to the 3-fold symmetry of the PESs, there are three equivalent conical intersections of the latter kind. The formation and disappearance of slits in the vector fields presented in Fig. 1 coincide exactly with these additional conical intersections. Of course, for $n = 3$, the additional conical intersections are known since a long time as was shown in Ref. 6. In the present work, we show that this is a more general feature of C_{nv} systems, at least when modeled in the way described above. Whenever the two used expansion terms are of different orders, this corresponds to the existence of additional conical intersections. The radius r_{CI} where these additional conical intersections occur corresponds to the real positive roots of

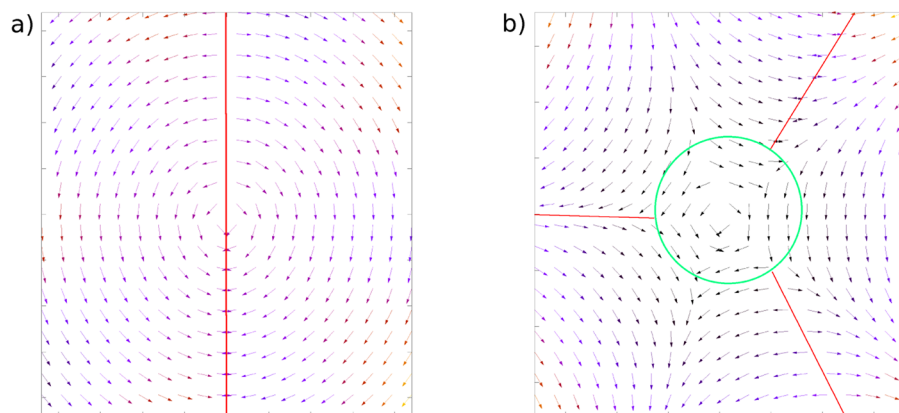


FIG. 2. Vector field of the eigenvectors corresponding to the lower adiabatic PES plotted in the plane of the $Q_{\beta x}$ and $Q_{\beta y}$ coordinates. (a) shows the inner region for C_{5v} ($E_1 \otimes e_1$). (b) presents the outer region for the same case. The green circle indicates the radius separating the inner from outer region.

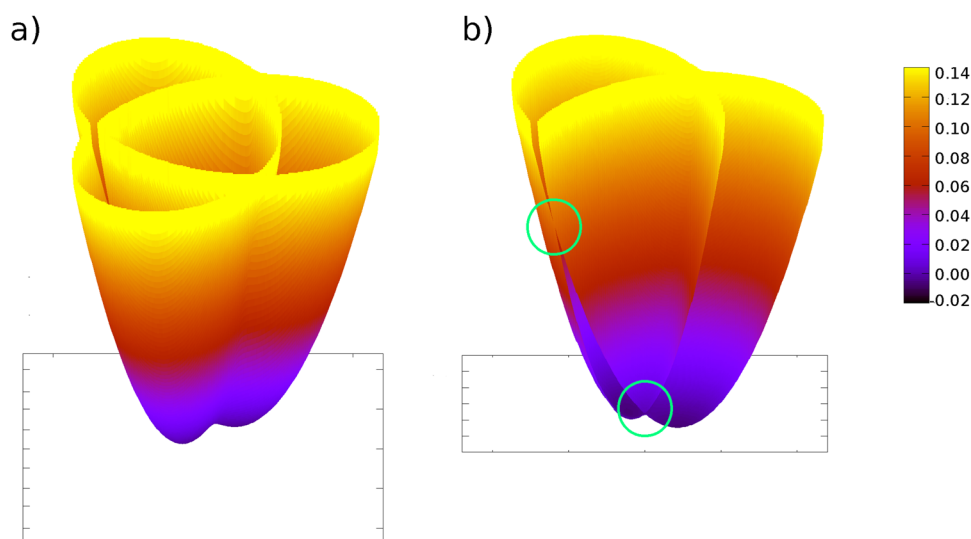


FIG. 3. Adiabatic PESs for $n = 3$ in the two-dimensional space spanned by Q_x and Q_y . (a) illustrates the 3-fold symmetry. (b) presents a view cutting through the origin and clearly showing the conical intersections at the origin and for larger r at high energy (marked by green circles). Color coded energies in arbitrary units.

$P_{n\alpha}(Q_{\beta+}, Q_{\beta-})$. For example, as modeled here for the case $n = 3$, the distance of the additional conical intersection from the symmetry point is simply $r_{CI} = \frac{c_1}{c_2}$ (in agreement with Ref. 6) and for $n = 5$ $E_1 \otimes e_2$ ($E_2 \otimes e_1$), it is $r_{CI} = \sqrt[3]{\frac{c_1}{c_2}}$, where c_1 and c_2 refer to the two expansion coefficients. The radii separating inner and outer regions for all systems treated here can be found approximately by solving for the roots of the functions given in the last column of Table I in which the general totally symmetric expansion functions $f_{k\pm}^\alpha(r_\beta^2)$ [see Eq. (17)] and their derivatives are used.

The existence of additional conical intersections induces two effects. First of all, the additional conical intersections induce local geometric phases, which may play an important role in wave packet propagations. Second, the additional conical intersections will lift the effect of the intersection at the symmetry point (or in general other *inner* intersections). Therefore, the additional conical intersections will change the properties of the vibronic eigenstates. This has been observed before for $n = 3$.^{6,11,12} An odd number of additional conical intersections on a ring around the symmetry point will flip the behavior such that if in the inside of the ring there is no geometric phase, at the outside there will be one and vice versa. An even number of additional conical intersections will not induce such a flip of the properties.

The above discussion gives a clear picture of what happens to the system in the two limiting cases with the wave function either entirely located in the inner or outer region, respectively. However, this clear picture is lost if the wave function extends significantly beyond the dividing line and thus probes the additional conical intersections only partially. In such a case, the impact of the conical intersections and corresponding local geometric phases is not well-defined and the concept of the GPE reaches its limits as a useful concept.

IV. GEOMETRIC PHASE AND SPECTROSCOPY

It has been recognized early on that the existence of a geometric phase has an impact on the vibronic ground state of a Jahn-Teller

system.^{2,3} Model systems with linear and quadratic coupling terms have been shown to have a ground state of E vibronic symmetry in general. An elegant proof for this was given by Ham.⁵ However, it has been shown that the ordering of the first two states switches from E/A (meaning E lower in energy than A) to A/E above a certain value of the quadratic coupling constant.^{11,12} This is due to the fact that for strong quadratic and weak linear coupling, the wave function is not localized in the inner region but extends considerably to the outer region. Thus, it probes four instead of one conical intersection. Furthermore, Ham showed that an alternating pattern should be expected for increasing excitation quanta. We recently found in our investigation of the vibronic eigenstates of the nitrate radical (NO_3) a more complicated and rather intriguing pattern of the vibronic level structure and proposed an explanation for these observations.¹⁴ Here, we generalize these findings beyond C_{3v} and D_{3h} systems.²⁵

As discussed in Sec. III, an n -fold principal axis induces n/m equivalent minima on the lower sheet of the adiabatic PESs for any $E_\alpha \otimes e_\beta$ JT system (m depends on n and β and usually $m = 1$). The local environment around these minima shows a lower symmetry than the symmetry of the full system and if the wells are sufficiently deep the wave function will “localize” (i.e., will have a significantly increased density) in these wells. This is essentially equivalent to the Jahn-Teller theorem stating that the equilibrium geometry is distorted from its highest possible symmetry.²⁶ The molecular vibrations can be conceived as small oscillations of the atoms around their respective equilibrium positions. However, these equilibrium positions refer to one of the equivalent local minima, and the PES in the vicinity of these minima only shows the reduced local symmetry. Therefore, vibrations formally belonging to a degenerate e_β mode in the two dimensional isotropic harmonic oscillator will not degenerate in the local symmetry and thus the corresponding vibronic levels will split. These local vibrations are equivalent for the n/m minima and must be symmetrized according to the global symmetry. This leads to sets of n/m vibronic states for each kind of local vibration, and these

vibronic states transform as irreducible representations of the global symmetry group. If the barriers between the local minima are high enough, the vibronic states form tunneling sets and the corresponding tunneling splittings depend on the well depth and the barrier height between the wells. For more shallow wells or higher excitations, the vibronic level energies may be above the barriers but the general structure of what we call “tunneling sets” or “tunneling multiplets” remains because this is simply a consequence of the global symmetry of the system and of the equivalent potential wells.

This situation can be approximated and analyzed very efficiently with a next neighbor or Hückel model. The n -fold symmetry axis of any C_{nv} point group corresponds to a rotation operator \hat{C}_n transforming one local state residing in one local minimum into the corresponding local state residing in the neighboring PES well. If we further assume that the local states can only interfere with the ones in the neighboring wells, we can write the Schrödinger equation in the next neighbor approximation as

$$\begin{pmatrix} a-E & b & 0 & 0 & \dots & b \\ b & a-E & b & 0 & \dots & 0 \\ 0 & b & a-E & b & \dots & 0 \\ \vdots & & & & \ddots & \vdots \\ b & 0 & 0 & \dots & b & a-E \end{pmatrix} \begin{pmatrix} c_1 \\ c_2 \\ c_3 \\ \vdots \\ c_n \end{pmatrix} = \begin{pmatrix} 0 \\ 0 \\ 0 \\ \vdots \\ 0 \end{pmatrix}. \quad (26)$$

Here, a stands for the expectation value of the vibrational Hamiltonian over a purely local eigenstate and b for the integral corresponding to the tunneling interaction with the next neighbor local state. This yields the relation

$$b c_{j-1} + (a-E) c_j + b c_{j+1} = 0, \quad \text{with } 1 < j < n-1. \quad (27)$$

The elements of each eigenvector, c_{j-1} , c_j , and c_{j+1} , are related to each other strictly by symmetry. The resulting n eigenvalues are simply

$$E_k = a + 2b \cos\left(\frac{2\pi k}{n}\right), \quad k = 0, 1, \dots, n-1. \quad (28)$$

For example, for $n = 3$, the eigenvalues would be $a + 2b$ (A), $a - b$ (E), and $b < 0$ for the ground state of systems without the GPE. Thus, the expected level ordering would be (A) below (E). The ordering of the tunneling multiplets only depends on the sign of b , which is a tunneling probability determined from the localized basis functions.

The parameters a and b are determined following the ideas of Wallace developed for the band theory of graphite.²⁷ As an example, the model for C_{3v} is considered, but the results are general and the conclusions for the other point groups are to be obtained by analogy. For the calculation of a and b , the adiabatic potential of the electronic ground state (lower adiabatic PES sheet) is expanded in a Taylor series around a local minimum, using the planar polar coordinates r and ϕ . This yields

$$\begin{aligned} V_-^{ad} &= r^2 - \sqrt{(c_{11}r)^2 + (c_{22}r^2)^2 + 2c_{11}c_{22}r^3 \cos(3\phi)} \\ &= r^2 - (c_{11}r + c_{22}r^2) \sqrt{1 + \frac{2c_{11}c_{22}r}{(c_{11} + c_{22}r)^2} (\cos(3\phi) - 1)}, \end{aligned}$$

which is further approximated by

$$\begin{aligned} V_-^{ad} &\approx r^2 - c_{11}r - c_{22}r^2 - \frac{c_{11}c_{22}r}{c_{11} + c_{22}r} (\cos(3\phi) - 1) \\ &\approx (1 - c_{22}) \left(r - \frac{c_{11}}{2 - 2c_{22}} \right)^2 + \frac{9}{2} \frac{c_{11}c_{22}r^2}{c_{11} + c_{22}r} \phi^2 - \frac{c_{11}^2}{4 - 4c_{22}}. \end{aligned} \quad (29)$$

Defining

$$r_0 = \frac{c_{11}}{2 - 2c_{22}}, \quad (30a)$$

$$\omega_r = \sqrt{2 - 2c_{22}}, \quad (30b)$$

$$I\omega_\phi = \sqrt{9 \frac{c_{11}c_{22}r_0^2}{c_{11} + c_{22}r_0}}, \quad (30c)$$

and

$$V_0 = -\frac{c_{11}^2}{4 - 4c_{22}} \quad (30d)$$

yields the final expansion and definition of the local potential $V^{local}(r, \phi)$ limited to a single well around $\phi = 0$,

$$V_-^{ad} \approx \frac{1}{2} \omega_r (r - r_0)^2 + \frac{1}{2} I\omega_\phi \phi^2 + V_0 \equiv V^{local}(r, \phi). \quad (31)$$

The local Hamiltonian is defined in terms of the local potential as

$$H^{local} = T + V^{local}, \quad (32)$$

where T represents the kinetic energy. This local Hamiltonian corresponds to a two-dimensional harmonic oscillator. The solutions to this system are composed of the well-known one-dimensional harmonic oscillator functions $\Phi_{i, mass, frequency}^{HO}(x)$,

$$\Psi_{p_r, p_t}^{local}(r, \phi) = \exp\left(\frac{2i\phi}{3}\right) \Phi_{p_r, 1, \omega_r}^{HO}(r - r_0) \Phi_{p_t, r_0^2, \omega_\phi}^{HO}(\phi). \quad (33)$$

The quantum numbers p_r and p_t correspond to the radial and tangential motion, respectively. In addition, this solution contains a factor $\exp(\frac{2i\phi}{3})$ accounting for the geometric phase directly induced by the fact that C_{3v} is fermionic. When considering a bosonic case, this geometric phase factor is absent. For each combination of p_r and p_t , the three local wave functions $\Psi_{p_r, p_t}^{local}(r, \phi)$, $\Psi_{p_r, p_t}^{local}(r, \phi - \frac{2\pi}{3})$, and $\Psi_{p_r, p_t}^{local}(r, \phi + \frac{2\pi}{3})$ are the solution for each local well, respectively. Each of these triplets of wave functions with the same p_r and p_t forms a basis for a Hückel model like the one given in Eq. (26). The diagonal elements a_{p_r, p_t} are approximated as the local energies,

$$a_{p_r, p_t} = \omega_r \left(p_r + \frac{1}{2} \right) + \omega_\phi \left(p_t + \frac{1}{2} \right) + V_0. \quad (34)$$

The off-diagonal elements of the Hückel matrix are given by the integral

$$b_{p_r, p_t} = \int_0^\infty dr \int_{-\pi}^\pi d\phi \Psi_{p_r, p_t}^{local}(r, \phi + \frac{2\pi}{3}) H \Psi_{p_r, p_t}^{local}(r, \phi). \quad (35)$$

Replacing H by $T + V^{local} + V - V^{local}$ yields

$$\begin{aligned} b_{p_r, p_t} &= a_{p_r, p_t} S_{p_r, p_t} + \int_0^\infty dr \int_{-\pi}^\pi d\phi \Psi_{p_r, p_t}^{local}(r, \phi + \frac{2\pi}{3}) \\ &\quad \times (V - V^{local}) \Psi_{p_r, p_t}^{local}(r, \phi), \end{aligned} \quad (36)$$

where S_{p_r, p_t} is the overlap between two consecutive local wave functions. As usual in the Hückel approximation, this term is neglected such that

$$b_{p_r, p_t} \approx \int_0^\infty dr \int_{-\pi}^\pi d\phi \Psi_{p_r, p_t}^{local} \left(r, \phi + \frac{2\pi}{3} \right) (V - V^{local}) \cdot \Psi_{p_r, p_t}^{local} (r, \phi). \quad (37)$$

Taking into account the geometric phase factors of the local wave functions, the equation simplifies to

$$b_{p_r, p_t} \approx - \int_0^\infty dr \int_{-\pi}^\pi d\phi |\Phi_{p_r, 1, \omega_r}(r - r_0)|^2 \Phi_{p_t, r_0^2, \omega_\phi} \left(\phi + \frac{2\pi}{3} \right) \times \Phi_{p_t, r_0^2, \omega_\phi}(\phi) (V - V^{local}). \quad (38)$$

Because the difference $V - V^{local}$ is always negative, the sign of this integral does only depend on the sign of the product $o = \Phi_{p_t, r_0^2, \omega_\phi} \left(\phi + \frac{2\pi}{3} \right) \Phi_{p_t, r_0^2, \omega_\phi}(\phi)$. The product of these local angular wave functions is positive for even p_t and negative for odd p_t . (This holds strictly at least for the lowest few vibronic levels before the normal mode picture becomes invalid anyway.) The graphical representation given in Fig. 4 clearly shows the link between the sign of b_{p_r, p_t} and the parity of p_t of the local oscillator depending on ϕ . This implies that $b_{p_r, p_t} > 0$ for even p_t and $b_{p_r, p_t} < 0$ for odd p_t . Since the level ordering in each tunneling multiplet is ruled by the sign of b_{p_r, p_t} , we conclude that each tangential excitation inverts the order of the tunneling multiplet with respect to the ordering of the multiplet with one less quanta along ϕ . For C_{3v} , this means that the ground state multiplet is E under A and the multiplet corresponding to the first local tangential excitation is A below E and so on.

The argument for different groups C_{nv} is entirely equivalent keeping in mind that for bosonic cases, the negative sign in Eq. (38) is absent because no geometric phase occurs in this case (for a detailed explanation, see Sec. II B). In a bosonic case, b_{p_r, p_t} is negative for even p_t and positive for odd p_t , while in a fermionic case, b_{p_r, p_t} is positive for even p_t and negative for odd p_t . This explains why fermionic and bosonic cases show opposite behavior regarding the level ordering. The results of the Hückel-like model holds

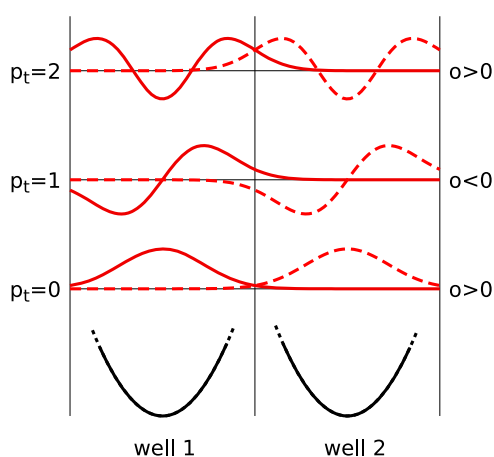


FIG. 4. Local angular wave functions and local potential of two wells in the Hückel model. The product o of the ground state and the second excited state is positive, but the product o of the first excited states is negative.

true even if the energy of the wave function is above the tangential barriers. The tunneling constant b_{p_r, p_t} becomes large, but the general structure is preserved. The simple picture is gradually destroyed if Fermi resonances are present. These occur if the spectrum becomes dense and states of the same symmetry start to be close, which usually happens in all multimode systems beyond the first few quanta of excitation.

In the following, we first will demonstrate this effect by numerical simulations²⁸ for $n = 3$ before discussing higher n . The two leading coupling terms for $n = 3$ are of first and second order (see Table I), and only the combination of the two results in the three equivalent wells. The numerical values used in the following ensure that the densities of the vibronic wave functions outside the inner region are negligible and thus that the inner region characteristics are the only ones relevant for the analysis. The leading first order term induces a geometric phase. The vibrationless ground state of a molecule sitting in one of the wells shows no node of the wave function within the well. However, the global symmetrization over the three wells leads to a vibronic ground state of E symmetry and an excited state of A_2 symmetry together forming a tunneling triplet. It might appear counter-intuitive at first that the vibrationless ground state shows nodes in the wave function. However, these nodes appear between the equivalent wells rather than within the wells. The ordering of E below A as well as the A_2 symmetry of the excited tunneling component is a consequence of the geometric phase effect. The situation is visualized in Fig. 5 where the densities of the vibronic wave functions numerically computed using a prototypical model are plotted.

The densities of the two components of the E state show the expected lack of symmetry with respect to C_3 rotation and cannot be easily interpreted. By contrast, the sum of these two densities shows the rotational symmetry and also demonstrates that the wave function is nodefree within each of the three potential wells. Summing up the E components also allows us to identify the tunneling sets of vibronic states which share the same local vibration as the comparison of Figs. 5(c) and 5(d) demonstrates.

Next, we consider vibrational excitations. It is customary to label the vibrational modes according to the global symmetry. Therefore, it is helpful to map the irreps of the modes in global symmetry onto the corresponding irreps of the local symmetry. The degenerate e modes of global symmetry are of particular interest as these map onto two different irreps in the local symmetry, namely, symmetric (a') or antisymmetric (a''), with respect to the vertical mirror planes σ_v . If the polar coordinate representation of the Hamiltonian equations (4) and (5) is used, the first case would correspond to a radial excitation while the second case would correspond to a tangential excitation. It is obvious that the PES in the vicinity of the equivalent PES minima is rather different in radial and tangential directions, respectively, and this leads to a splitting of the vibronic levels depending on the local excitation direction. Furthermore, the tangential excitation is connected with the tunneling probability (see above), while the radial excitation is not. As a consequence, odd quanta of tangential excitation induce a sign change in the tunneling parameter of the simple next-neighbor model presented above and in our previous study of NO_3 ¹⁴ and thus the order within the tunneling multiplets is inverted. By contrast, any excitation in radial direction as well as even quanta in the tangential mode has no effect on the tunneling parameter thus not affecting the ordering.

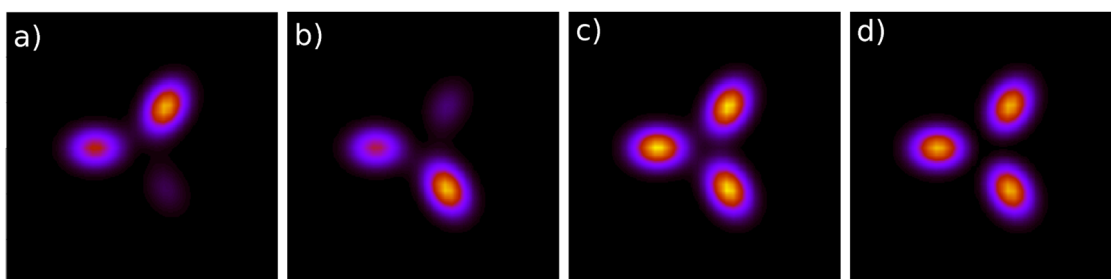


FIG. 5. Density of vibronic state wave functions for $n = 3$ plotted in the Q_x, Q_y plane. (a) First component of the E ground state, (b) second component of the E ground state, (c) sum of first and second components of the E ground state, and (d) A_2 excited tunneling state.

The behavior of the energy levels can be summarized by simple rules. It is customary to interpret vibronic spectra in terms of normal modes transforming as e . In a local isolated deformed oscillator, these normal modes transform like a' and a'' with respect to the local symmetry group C_s . A single radial excitation transforms like a' , and a single tangential excitation transforms like a'' . Symmetrizing these local excitations with respect to the global symmetry group C_{3v} yields the tunneling triplets. This scheme is represented in Fig. 6 for a formally single e excitation. The ordering of the tunneling multiplets depends on the number of tangential quanta of each state. The set ($a' C_s$) corresponding to radial excitation is ordered E/A as in the ground state. By contrast, the set ($a'' C_s$) corresponding to a single tangential excitation is inverted with respect to the ground state pattern and the ordering is A/E . The odd tangential excitation also causes the nondegenerate state to be A_1 rather than A_2 . The construction principle of the vibronic level structure now is clear and can be applied to formally higher excitations in the e modes as well. For example, a double excitation (e)² first leads to a threefold splitting of the levels because the different combinatorial possibilities of the excitations are different for (e_r)², (e_t)², and (e_r)¹(e_t)¹, where e_r and e_t refer to radial and tangential motions, respectively. Each of the three types of local vibrations will result in a tunneling triplet and the level ordering of

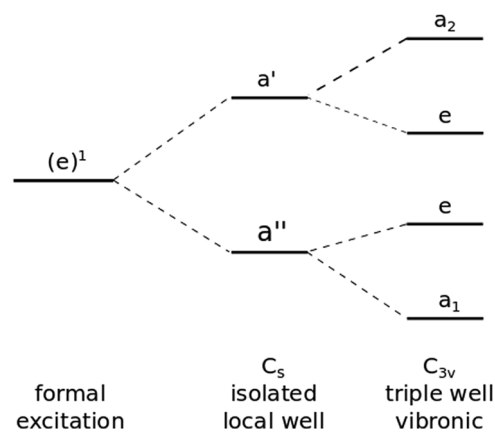


FIG. 6. Vibronic level structure of a formal (e)¹ excitation for $n = 3$.

the first two cases (even tangential quanta) will be E/A , while the third case corresponds to odd tangential quanta and thus results in A/E level ordering. This scheme holds for cases for which the lower adiabatic PES sheet shows reasonably pronounced multiwell character.

The behavior of the two different kinds of triplets in C_{3v} (resulting from radial or tangential excitation) with respect to the coupling parameters can be studied systematically, which is illustrated in Fig. 7. Setting linear and quadratic coupling to zero results in an isotropic harmonic oscillator for each of the two electronic components. In this isotropic two dimensional harmonic oscillator, the first few vibronic energy levels are 2-, 4-, 6-, and 8-fold degenerate. Using the irreps of the C_{3v} symmetry group, the ground state is of e symmetry, the first excited state transforms like e , a_1 , and a_2 , the second excited state transforms like e , e , a_1 , a_2 , and so on. The linear coupling term distorts the isotropic harmonic oscillator to the well-known “Mexican hat” shape. As a result, some degeneracies of the isotropic oscillator are lifted. The split energy levels are always twofold degenerate and correspond to the $\pm\lambda/2$ values of the vibronic angular momentum since the cylindrical symmetry is still preserved. As shown in the left half of Fig. 7, the splitting becomes stronger for increasing linear coupling strength. Note, however, that all states can be classified in terms of the C_{3v} irreducible representations and can be grouped into the aforementioned tunneling triplets. For a triplet corresponding to even tangential quanta (black lines in Fig. 7), the e state is always lower in energy than the a_2 state. Examples are the ground state, the states labeled $r^1 t^0$, $r^2 t^0$, and $r^0 t^2$. The state assignments in terms of radial and tangential excitations are given as labels in the right half of Fig. 7. For states corresponding to odd tangential quanta (red lines in Fig. 7), the a_1 part of a triplet is always lower in energy than the corresponding e state. This is true even if the spectrum becomes very dense. When a quadratic term is added, the 2-fold degeneracies of the a_1 and a_2 energies are lifted as shown in the right half of Fig. 7 where the quadratic coupling is increased for a given linear coupling value. In a vibronic coupling model with a linear and a weak quadratic coupling, the splitting of the triplets is quite large as seen near the center of Fig. 7. Therefore, different triplets overlap, but nevertheless, the ordering of each triplet stays invariant (a_2 above e or e above a_1 depending on the number of tangential quanta, i.e., solid below dashed lines for black and dashed below solid for red in Fig. 7). For increasing quadratic coupling, the splitting between the triplet components decreases and its existence becomes more obvious (see near 0.5 to

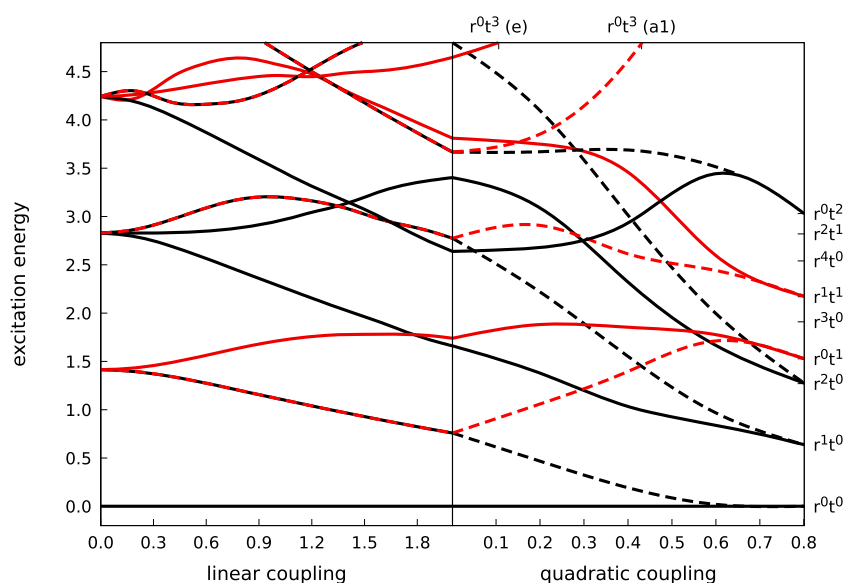


FIG. 7. Vibronic excitation energies of a C_{3v} symmetric JT system. Couplings and energies are given relative to the harmonic constant. For the left half of this figure, the quadratic coupling is set to 0 and the linear coupling varies from 0 to 2. In the right half, the linear coupling is set to 2 and the quadratic coupling is varied from 0 to 0.8. Vibronic states with e symmetry are drawn as solid lines, and vibronic levels of a_1 or a_2 symmetry are marked with dashed lines. Fermionic states are indicated by black lines, and bosonic states are given in red. The states are labeled by their excitation assignment on the right border.

0.6 of quadratic coupling in Fig. 7). The triplets start to be “true” tunneling triplets of the corresponding triple well system. If the quadratic coupling is very strong, the triple well effectively becomes a collection of three isolated oscillators. In this case, tunneling is unlikely and therefore the triplets become essentially degenerate as seen at the right border of Fig. 7. It turns out that for reasonably strong quadratic JT coupling, the Hückel-like picture is more adequate than the picture of a perturbed isotropic harmonic oscillator because the tangential multiwell structure of the potential becomes important.

A confirmation of the predicted patterns is again obtained by numerical model calculations and the analysis of the densities of the vibronic eigenstates. The characteristic densities of the lowest excited vibronic states obtained from a numerical model in which the relevant part of the vibronic wave functions samples mostly the *inner* region are presented in Fig. 8.

The nodal structure of the vibronic wave functions is clearly visible, and radial and tangential excitations can be distinguished easily. The states belonging to a specific tunneling triplet are found by comparing the sum of densities of the E state components with the density of the associated A state. This yields the specific level ordering for each tunneling triplet which is also given in Fig. 8. Figures 8(a), 8(c), 8(e), and 8(h) show states with radial excitations exclusively. The corresponding levels are all ordered E/A_2 like the ground state tunneling triplet because there are no odd tangential quanta. Figures 8(b) and 8(g) show states with tangential excitations exclusively. The states with a single tangential excitation correspond to a level ordering of A_1/E , while the states with a double tangential excitation yield E/A_2 as predicted. Finally, Figs. 8(d) and 8(f) show states with a single tangential node combined with one or two radial nodes, respectively. In both cases, the observed level ordering is A_1/E in agreement with our theoretical prediction. The numerical simulations demonstrate clearly that the theory for the ordering within the tunneling sets outlined above holds for the low lying vibronic states. Note however that the energetic splitting between

different tunneling sets will depend on the specific system. Finally, the above findings hold for low lying states. At higher energies and for real multimode systems, this clear picture will be lost gradually as assignments using excitation quantum numbers will become impossible due to vibronic state interactions (e.g., Fermi resonances). This is a general problem for all multimode vibrational assignments because of the rapidly increasing density of states, which is not a special property of the JT systems studied here. Clear assignments are usually not possible beyond the first few excitation quanta.

Next, the case $n = 4$ is considered for which the two leading coupling terms are of second order, and thus no geometric phase is induced by the PES. Therefore, the vibronic ground state of the system is a nondegenerate A_1 state followed by E and B_1 forming the lowest tunneling quartet. This is indeed observed in our numerical simulations which also include higher excitations. The densities of the first four tunneling sets are displayed in Fig. 9. The first local excitation is found to be a radial one, and thus the same ordering $A_1/E/B_1$ is observed for the vibronic states corresponding to this tunneling set. By contrast, the second single excitation is the tangential one. This results in a tunneling set with a state ordering of $B_2/E/A_2$ which again shows a nondegenerate lowest component. In this case, the inversion of the tunneling multiplet only affects the nondegenerate states exchanging A and B as well as “1” and “2,” respectively. The next set refers to a double excitation in the radial direction for which again the order $A_1/E/B_1$ is expected. Instead, an ordering of $E/A_1/B_1$ is observed in the numerical results. The reason for this apparently is that the four equivalent wells of our numerical example on the lower adiabatic PES sheet are very shallow and a double excitation is already sufficiently above the origin energy at the degeneracy point so that due to the very high density of vibronic states the simple reasoning used above becomes insufficient. State-state interactions (Fermi resonances) can lead to different orderings within the tunneling sets because the density of states strongly increases with energy and thus it is more likely that states of

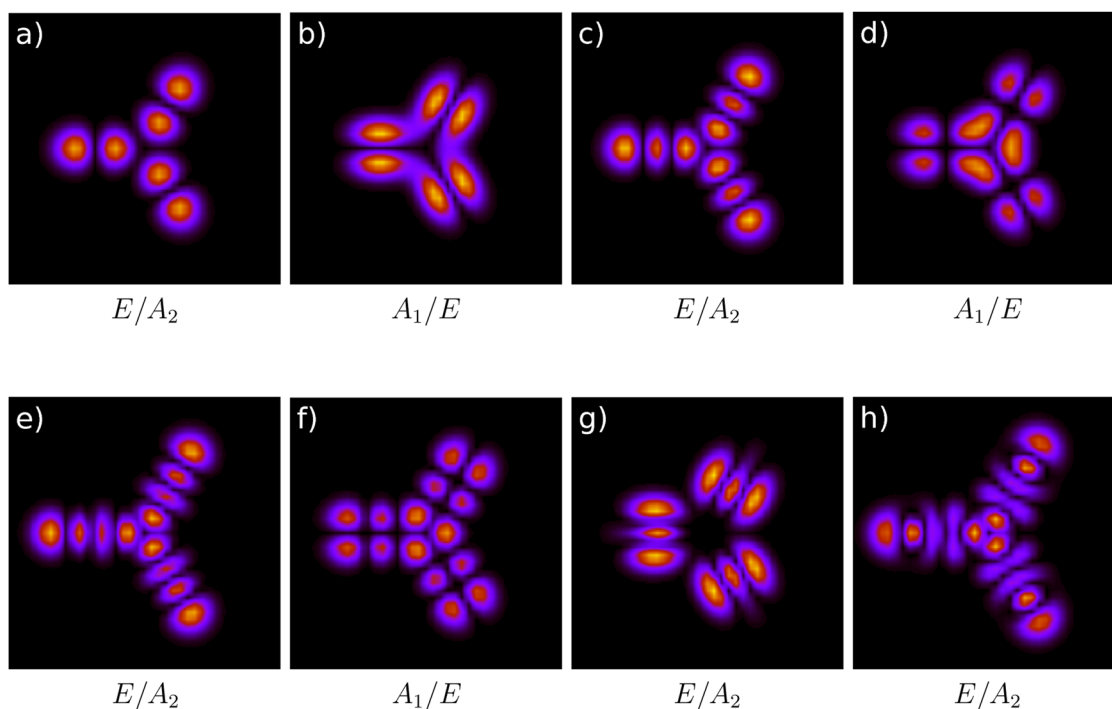


FIG. 8. Density of excited vibronic state wave functions for $n = 3$ plotted in the Q_x, Q_y plane together with the symmetry labels of the energy ordered multiplets. The local excitations are $r^1 t^0$ (a), $r^0 t^1$ (b), $r^2 t^0$ (c), $r^1 t^1$ (d), $r^3 t^0$ (e), $r^2 t^1$ (f), $r^0 t^2$ (g), and $r^4 t^0$ (h).

the same symmetry are in energetic proximity and mix. In fact, the E states show significant mixing with a higher E state in the present example.

The C_{5v} point group is the first case for which two different two-dimensional irreps E_1 and E_2 exist, and thus the situation is considerably more complex than for the previous examples. The leading terms in the diabatic PES models are first order for $E_1 \otimes e_2$ and $E_2 \otimes e_1$ and second order for $E_1 \otimes e_1$ and $E_2 \otimes e_2$. Consequently, the first two combinations will behave fermionic due to the existence of a GPE, while the latter two combinations will have bosonic properties. The effects on the vibronic eigenstates are

displayed in Fig. 10. The first and obvious observation is that the ground state is of A_2 symmetry in the bosonic case [see Fig. 10(a)] and of E symmetry in the fermionic combination [see Fig. 10(e)]. The first two computed excitations in the $E_1 \otimes e_1$ case correspond to radial local excitations, and thus the ordering of the tunneling quintet of $A_2/E_1/E_2$ remains the same. The third local excitation puts a single quantum into the tangential mode and thus leads to an inversion of the tunneling quintet resulting in a level ordering of $E_2/E_1/A_1$. When analyzing the isomorphic case $E_2 \otimes e_2$, the only difference with respect to $E_1 \otimes e_1$ is that the two vibronic E levels E_1 and E_2 are interchanged. As expected, the numerical results for the

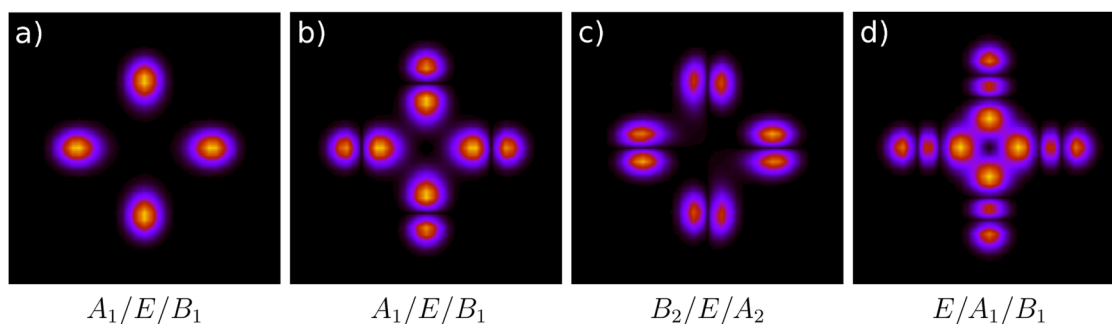


FIG. 9. Density of low lying vibronic state wave functions for $n = 4$ plotted in the Q_x, Q_y plane. The local excitations are $r^0 t^0$ (a), $r^1 t^0$ (b), $r^0 t^1$ (c), and $r^2 t^0$ (d).

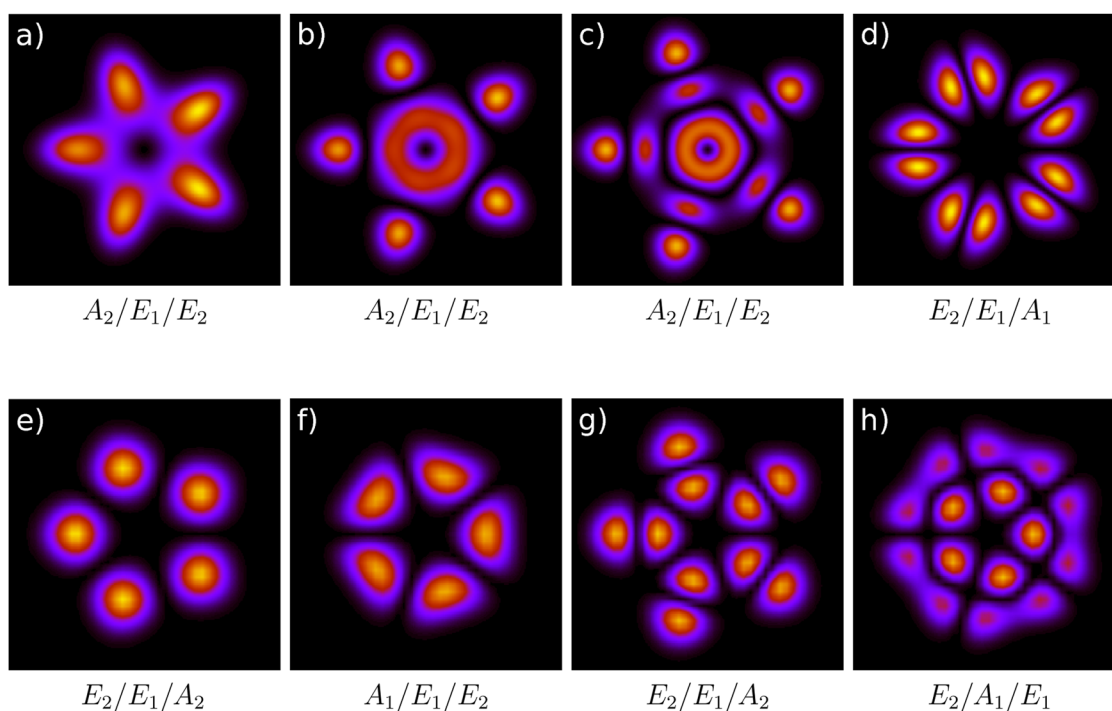


FIG. 10. Density of vibronic state wave functions plotted for $n = 5$ in the Q_x, Q_y plane. (a)–(d) show the $E_1 \otimes e_1$ case; (e)–(h) show the $E_2 \otimes e_1$ case. The local excitations for the $E_1 \otimes e_1$ case are $r^0 t^0$ (a), $r^1 t^0$ (b), $r^2 t^0$ (c), and $r^0 t^1$ (d). The local excitations for the $E_2 \otimes e_1$ case are $r^0 t^0$ (e), $r^0 t^1$ (f), $r^1 t^0$ (g), and $r^1 t^1$ (h).

$E_2 \otimes e_1$ case show a different behavior. The vibronic ground state is E_2 followed by E_1 and A_2 which form the first tunneling set. The first excitation corresponds to a single tangential local excitation and thus inverts the tunneling quintet leading to a level ordering of $A_1/E_1/E_2$. The second excited tunneling set is due to a single radial local excitation and thus has the same level ordering as the ground state, $E_2/E_1/A_2$. The next set of states corresponds to a combination of a single radial and a single tangential excitation in the local wells and thus leads to an inversion again, and would be expected to result in the level ordering $A_1/E_1/E_2$. By contrast, the observed level ordering in our numerical example is $E_2/A_1/E_1$ because the E_2 state is lowered in energy by an interaction with another E_2 level nearby.

The symmetry group C_{6v} provides an interesting new situation because it is the first in the C_{nv} series to contain a non-Abelian subgroup, namely, C_{3v} , which is the most basic fermionic case of a JT system. In addition, C_{6v} has two 2-dimensional representations E_1 and E_2 leading to four different JT cases. $E_1 \otimes e_1$ and $E_2 \otimes e_1$ are bosonic due to a leading coupling term of second order (see Table I). The other two cases $E_1 \otimes e_2$ and $E_2 \otimes e_2$ have a diabatic Hamiltonian isomorphic to that of C_{3v} , and thus the lower adiabatic PES sheet only has three equivalent minima resulting in tunneling triplets for the vibronic states. This is the first case where the n/m equivalent minima correspond to $m > 1$. The e_2 coordinates are symmetric with respect to \widehat{C}_2 rotation, and thus the

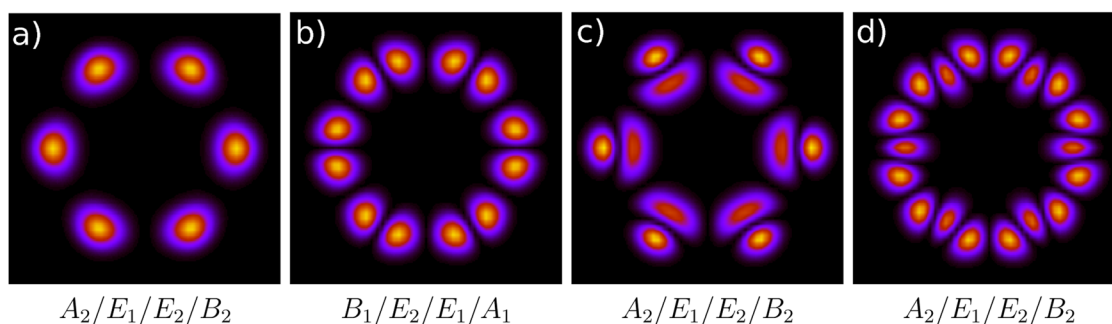


FIG. 11. Density of vibronic state wave functions plotted for $n = 6$ in the Q_x, Q_y plane for the $E_1 \otimes e_1$ case. The local excitations are $r^0 t^0$ (a), $r^0 t^1$ (b), $r^1 t^0$ (c), and $r^0 t^2$ (d).

seemingly missing three potential wells are excluded by the extra symmetry of the coordinates.²⁹ It is also shown easily using the fundamental properties of the C_{6v} irreps that the corresponding vibronic wave functions only can transform as A_1 , A_2 , or E_2 in this case.

The remaining two cases, $E_1 \otimes e_1$ and $E_2 \otimes e_1$, do not show the above idiosyncrasy and are analog to the two bosonic cases for C_{5v} but with the expected six equivalent minima. The corresponding vibronic densities are presented in Fig. 11 together with the level ordering of the tunneling sextets. The vibronic ground state is a nondegenerate A_2 level followed by the two degenerate states E_1

and E_2 and the highest level of the set transforms as B_2 . The densities of these four states do not show any node within the local PES wells. The next tunneling sextet corresponds to a single tangential excitation in the local wells, as shown clearly in Fig. 11(b). This changes the level ordering to $B_1/E_2/E_1/A_1$, similar to the corresponding $E_1 \otimes e_1$ case for C_{5v} [see Fig. 10(d)]. Figure 11(c) shows the next tunneling set corresponding to a single radial excitation in the local wells. Thus, the level ordering is found to be $A_2/E_1/E_2/B_2$. The states corresponding to Fig. 11(d) are due to a double tangential excitation in the local wells and thus again result in the pattern $A_2/E_1/E_2/B_2$.

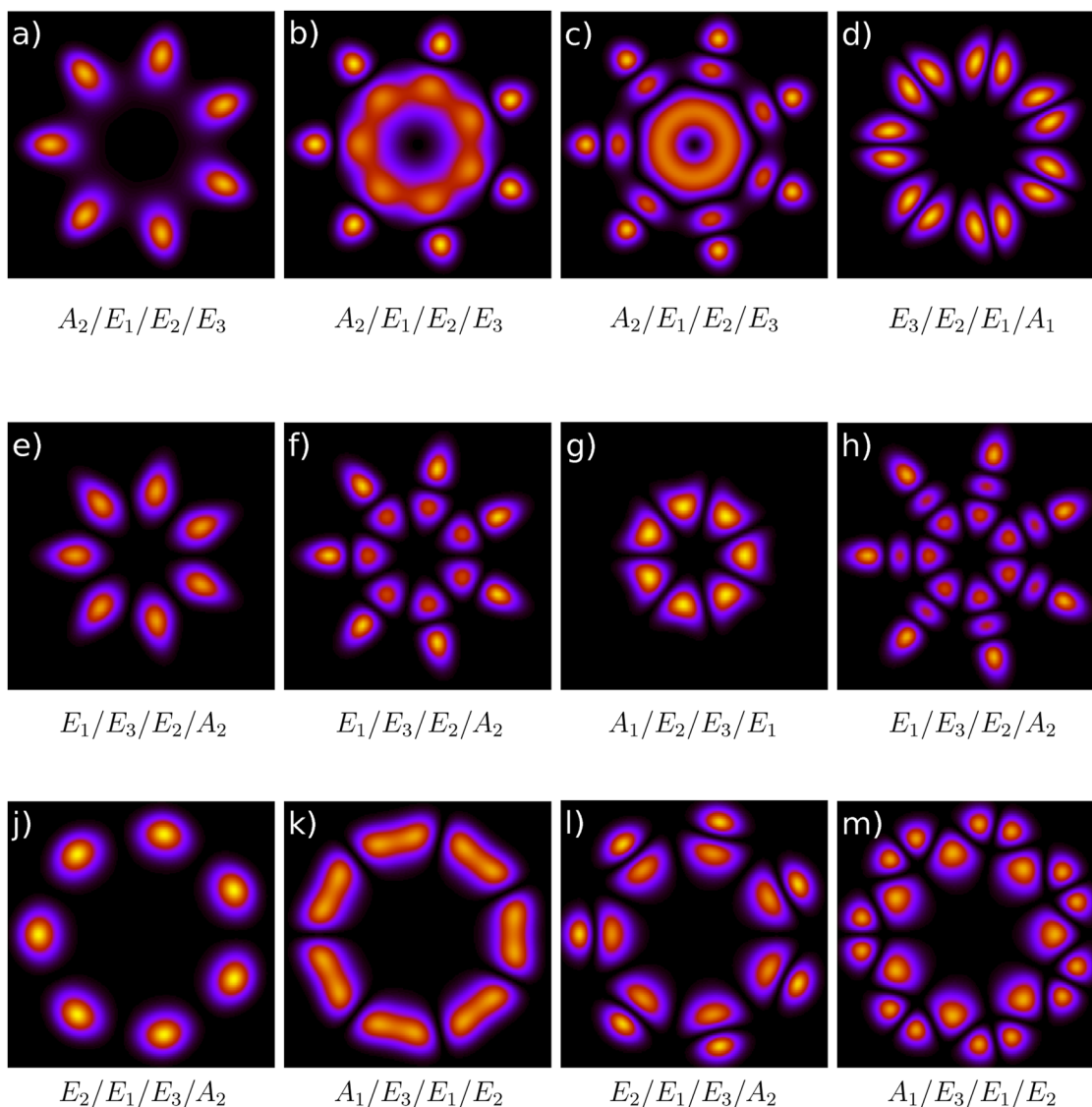


FIG. 12. Density of vibronic state wave functions plotted for $n = 7$ in the Q_x , Q_y plane. (a)–(d) show the $E_1 \otimes e_1$ case, (e)–(h) show the $E_1 \otimes e_2$ case, and (j)–(m) show the $E_1 \otimes e_3$ case. The local excitations for the $E_1 \otimes e_1$ case are $r^0 t^0$ (a), $r^1 t^0$ (b), $r^2 t^0$ (c), and $r^0 t^1$ (d). The local excitations for the $E_1 \otimes e_2$ case are $r^0 t^0$ (e), $r^1 t^0$ (f), $r^0 t^1$ (g), and $r^2 t^0$ (h). The local excitations for the $E_1 \otimes e_3$ case are $r^0 t^0$ (j), $r^0 t^1$ (k), $r^1 t^1$ (l), and $r^1 t^1$ (m).

C_{7v} is the first example for which three different E representations exist, leading to nine distinct $E_\alpha \otimes e_\beta$ combinations. The C_{7v} JT system also shows a new feature in the case of $E_1 \otimes e_3$, namely, a leading term in the diabatic Hamiltonian of third order. The vibronic state densities for the different combinations $E_1 \otimes e_1$, $E_1 \otimes e_2$, and $E_1 \otimes e_3$ are displayed in Fig. 12 for the ground and first few excited states. The $E_1 \otimes e_1$ case with a quadratic leading coupling term does not present a Berry phase. As a consequence, the level ordering for the ground state septet shows a nondegenerate lowest vibronic state (A_2) followed by three doubly degenerate levels ($E_1/E_2/E_3$) [see Fig. 12(a)]. The same ordering is obtained in Figs. 12(b) and 12(c)

which corresponds to a single and a double radial excitation. By contrast, in Fig. 12(d), a single tangential excitation induces an order of $E_3/E_2/E_1/A_1$ for the vibronic levels of the tunneling set. For both $E_1 \otimes e_2$ and $E_1 \otimes e_3$, a geometric phase effect is expected due to the odd power of the leading coupling term (see Table I). As a result, the lowest vibronic levels are doubly degenerate with an E_1 ground state for the case with a linear coupling term $E_1 \otimes e_2$ and a lowest level of E_2 in the case of the cubic leading term for $E_1 \otimes e_3$. In the case of $E_1 \otimes e_2$, the order $E_1/E_3/E_2/A_2$ obtained for the ground state multiplet [Fig. 12(e)] and for the radial excitations [Figs. 12(f) and 12(h)] is modified into $A_1/E_2/E_3/E_1$ when a single tangential excitation is present [Fig. 12(g)]. The third order

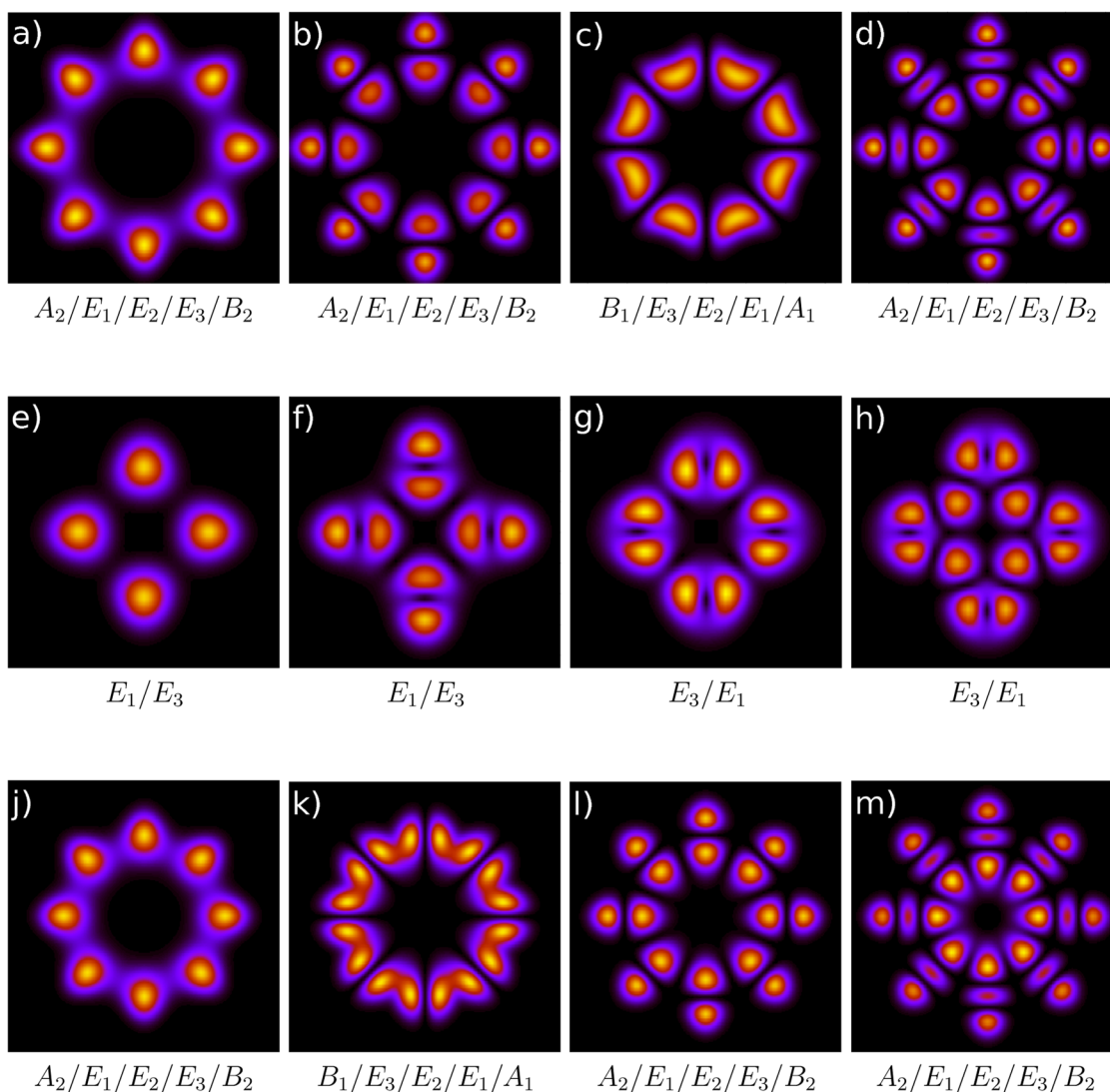


FIG. 13. Density of vibronic state wave functions plotted for $n = 8$ in the Q_x, Q_y plane. (a)–(d) show the $E_1 \otimes e_1$ case, (e)–(h) show the $E_1 \otimes e_2$ case, and (j)–(m) show the $E_2 \otimes e_1$ case. The local excitations for the $E_1 \otimes e_1$ case are $r^0 t^0$ (a), $r^1 t^0$ (b), $r^0 t^1$ (c), and $r^2 t^0$ (d). The local excitations for the $E_1 \otimes e_2$ case are $r^0 t^0$ (e), $r^1 t^0$ (f), $r^0 t^1$ (g), and $r^1 t^1$ (h). The local excitations for the $E_2 \otimes e_1$ case are $r^0 t^0$ (j), $r^0 t^1$ (k), $r^1 t^0$ (l), and $r^2 t^0$ (m).

leading term of $E_1 \otimes e_3$ results in an $E_2/E_1/E_3/A_2$ set of levels for the ground state multiplet and for multiplets corresponding to radial excitations [Figs. 12(j) and 12(l)] and in an $A_1/E_3/E_1/E_2$ level ordering when a single tangential excitation is involved [Figs. 12(k) and 12(m)].

Finally, we present the various cases for C_{8v} for which again three different E representations exist. The nine possible $E_\alpha \otimes e_\beta$ combinations yield four different Hamiltonians of which the $E_2 \otimes e_2$ one is isomorphic to the C_{4v} case. This is due to the fact that C_{4v} is a subgroup of C_{8v} and the situation is similar to the previously seen C_{6v} $E_{1,3} \otimes e_2$ cases. Distinct new cases are found for the isomorphic sets $\{E_{1,3} \otimes e_{1,3}\}$, $\{E_{1,3} \otimes e_2\}$, and $\{E_2 \otimes e_{1,3}\}$. Of these sets, only $\{E_{1,3} \otimes e_2\}$ shows an odd leading coupling term and thus a geometric phase due to the electronic Hamiltonian. The other two sets have even leading coupling terms, and thus the electronic Hamiltonian does not induce a GPE. A symmetry analysis of the vibronic eigenstates is performed using model simulations and the corresponding densities of the first few tunneling sets for the three new, distinct cases are displayed in Fig. 13. The ground state tunneling octet for the bosonic $E_1 \otimes e_1$ case shows a nondegenerate A_2 lowest level, as expected, followed by E_1 , E_2 , E_3 , and B_2 and thus is comparable to the findings for C_{7v} $E_1 \otimes e_1$. The next tunneling set is due to a single radial excitation, clearly visible in Fig. 13(b) and thus has the same level ordering as the ground state set. The first tangential excitation is found for the following tunneling set displayed in Fig. 13(c) and leads to a change of level ordering, which now reads $B_1/E_3/E_2/E_1/A_1$. Finally, a double radial excitation is found and, in agreement with the theoretical prediction, the observed level ordering is back to that of the ground state octet.

In contrast to the $E_1 \otimes e_1$ combination, the Hamiltonian of the $E_1 \otimes e_2$ system has a leading coupling term of odd (first) order and thus the electronic Hamiltonian induces a geometric phase in the ground state multiplet. Furthermore, the e_2 coordinates are invariant under C_2 rotation like in the case of the e_2 coordinates of C_{6v} . This causes the lower adiabatic PES sheet to support only four equivalent minima, and thus the vibronic states show up as tunneling quartets. It is also expected that the ground state should be doubly degenerate, which indeed is found in the numerical example. As seen in Figs. 13(e)–13(h), each tunneling quartet is composed of one E_1 and one E_3 state. The observed ordering is E_1/E_3 for all sets with no or even tangential quanta [Figs. 13(e) and 13(f)] and E_3/E_1 for all cases with odd tangential excitations [Figs. 13(g) and 13(h)].

Last but not least, the $E_2 \otimes e_1$ JT system is investigated for completeness. The leading coupling term of the electronic Hamiltonian is of fourth order, and thus the system is expected to show bosonic character. This is confirmed by the numerical simulation summarized in Figs. 13(j)–13(m). The ground state octet displayed in Fig. 13(j) and the tunneling sets corresponding to radial local excitations exclusively all result in a level ordering of $A_2/E_1/E_2/E_3/B_2$ in analogy to the other bosonic case $E_1 \otimes e_1$ [Figs. 13(a)–13(d)]. The single tangential local excitation visible in Fig. 13(k) leads to a set with a changed level ordering of $B_1/E_3/E_2/E_1/A_1$, also in agreement with the finding for the $E_1 \otimes e_1$ case [Fig. 13(c)].

The above numerical examples clearly confirm the general pattern following from the analytic analysis using the next neighbor approximation.

V. CONCLUSIONS

The quantum dynamics and the geometric phase effect (GPE) are studied in the present work for $E_\alpha \otimes e_\beta$ Jahn-Teller systems of C_{nv} groups with n varying from 3 to 8. The coupled potential energy surfaces (PESs), represented by analytical diabatic 2×2 matrices and derived here for all cases up to $n = 8$, all present at the symmetry coordinate origin a conical intersection or touching point depending on the n , α , and β values. The presence or absence of a GPE around this origin is directly linked to the polynomial order of the leading coupling term. The analytically unraveled characteristics of the coupled surfaces generally show an *inner* and an *outer* region separated by the location of additional conical intersections. These additional intersections do affect the conclusions about the presence or absence of a GPE when considering spatially extended vibronic wave functions for systems for which an odd number of additional conical intersections are present (thus mostly for odd n). By contrast, no change between inner and outer region results for systems with an even number of additional intersections (most of the cases with even n). These effects are studied analytically and are also visualized by plotting the vector fields of the eigenvectors of the diabatic Hamiltonian in the plane of the Cartesian e_β symmetry coordinates. The lines of sign change of the wave functions are clearly visible and are correlated with the order of the leading coupling term of the Hamiltonian. These topological slits are responsible for the presence or absence of the nontrivial topological phase in the adiabatic wave functions.

A second fundamental aspect is the presence of n/m equivalent minima on the lower adiabatic PES sheet for all C_{nv} $E_\alpha \otimes e_\beta$ systems (m depending on n and β). Such a topography leads to the existence of n/m -fold sets of vibronic eigenstates, which are studied in detail in the present work. These sets can be understood in terms of “local vibrations” within each of the local minima and a symmetrization over the equivalent PES wells. The local vibrations can be characterized as tangential or radial motions, respectively, when transformed to polar coordinates. This results in the formation of what we call vibronic tunneling sets, which can be obtained by a simple Hückel type model for weakly interacting local vibrations in a next neighbor approximation. The GPE has a clear impact on the level ordering of the tunneling multiplets, which furthermore depends on the type of local vibration. This effect is due to the sign of the tunneling parameter as shown analytically and changes the level ordering only if the local vibration corresponds to odd excitations of the tangential mode. Since the local environment within each well has a lowered “local symmetry,” the PES is distinctly different in the radial and tangential direction, respectively, leading to an energetic splitting between the corresponding tunneling sets. The GPE, together with the interpretation of local vibrations and symmetrization, is key for understanding the complicated vibronic spectra of real JT systems. The analysis of such spectra could also yield experimental evidence for the impact of the GPE. Any experiment which would provide reliable energy and symmetry data for all levels within a tunneling multiplet would be suitable to confirm the predicted effect of the nontrivial geometric phase on the level ordering.

The theoretical predictions obtained from the above analysis are tested using numerical models restricted to the two lowest

coupling terms for each case and determining the low energy range of the vibronic spectra for all C_{nv} $E_\alpha \otimes e_\beta$ JT systems up to $n = 8$. For all cases studied, the lower adiabatic PES sheet presents n/m equivalent wells as predicted. The signature of the GPE caused by the electronic Hamiltonian is that the vibronic ground state is a degenerate state of E symmetry. This is well known for C_{3v} and general linear vibronic coupling models. As shown here, this is always the case if the leading coupling term is of odd order and the vibronic wave function is dominated by the inner region of the PESs. For $n > 3$, we show that the degeneracy, and more precisely the irreducible representation, of the vibronic ground state does depend on n , α , and β . Furthermore, the numerical results confirm the theoretical interpretation of the tunneling multiplets in terms of symmetrized local vibrations. The different effect of local radial and tangential excitations, respectively, is clearly reflected in a change of the level ordering within each tunneling multiplet. The symmetry analysis of the numerical results provides a full characterization of the computed vibronic states for all cases treated. These results will be of significant help in the understanding of vibronic spectra of real systems.

ACKNOWLEDGMENTS

The authors are grateful for financial support via the PHC/DAAD grant PROCOPE (No. 40442PD) and the FCI (Fonds der Chemischen Industrie). Part of this work was also supported by the Deutsche Forschungsgemeinschaft (DFG).

REFERENCES

- ¹H. C. Longuet-Higgins, U. Öpik, M. H. L. Pryce, and R. A. Sack, *Proc. R. Soc. London, Ser. A* **244**, 1 (1958).
- ²R. Englman, *The Jahn-Teller Effect in Molecules and Crystals* (Wiley-Interscience, New York, 1972).
- ³M. C. M. O'Brien, *Proc. R. Soc. London, Ser. A* **281**, 323 (1964).
- ⁴C. A. Mead, *Chem. Phys.* **49**, 23 (1980).
- ⁵F. S. Ham, *Phys. Rev. Lett.* **58**, 725 (1987).
- ⁶J. W. Zwanziger and E. R. Grant, *J. Chem. Phys.* **87**, 2954 (1987).
- ⁷J. W. Zwanziger, M. Koenig, and A. Pines, *Annu. Rev. Phys. Chem.* **41**, 601 (1990).
- ⁸J. Schön and H. Köppel, *J. Chem. Phys.* **103**, 9292 (1995).
- ⁹C. A. Mead, *Rev. Mod. Phys.* **64**, 51 (1992).
- ¹⁰*Conical Intersections: Electronic Structure, Dynamics and Spectroscopy*, edited by W. Domcke, D. R. Yarkony, and H. Köppel (World Scientific, Singapore, 2004).
- ¹¹H. Koisumi and I. B. Bersuker, *Phys. Rev. Lett.* **83**, 3009 (1999).
- ¹²K. Pae and V. Hizhnyakov, *J. Chem. Phys.* **147**, 084107 (2017).
- ¹³W. Eisfeld, O. Vieuxmaire, and A. Viel, *J. Chem. Phys.* **140**, 224109 (2014).
- ¹⁴W. Eisfeld and A. Viel, *J. Chem. Phys.* **146**, 034303 (2017).
- ¹⁵A. Viel and W. Eisfeld, *Chem. Phys.* **509**, 81 (2018).
- ¹⁶A. Viel and W. Eisfeld, *J. Chem. Phys.* **120**, 4603 (2004).
- ¹⁷W. Eisfeld and A. Viel, *J. Chem. Phys.* **122**, 204317 (2005).
- ¹⁸D. Opalka and W. Domcke, *J. Chem. Phys.* **132**, 154108 (2010).
- ¹⁹S. Bhattacharyya, D. Opalka, L. V. Poluyanov, and W. Domcke, *J. Phys. Chem. A* **118**, 11962 (2014).
- ²⁰C. Roberston and G. A. Worth, *Chem. Phys.* **460**, 125 (2015).
- ²¹T. Zeng and I. Seidu, *Phys. Chem. Chem. Phys.* **19**, 11098 (2017).
- ²²E. Wigner and J. Griffin, *Group Theory and Its Application to the Quantum Mechanics of Atomic Spectra*, Pure and Applied Physics (Academic Press, 1959).
- ²³D. M. G. Williams and W. Eisfeld, *J. Chem. Phys.* **149**, 204106 (2018).
- ²⁴M. V. Berry, *Proc. R. Soc. London, Ser. A* **392**, 45 (1984).
- ²⁵Note: The general findings presented here for C_{nv} groups are easily extended to general D_{nh} groups. D_{nh} are direct product groups of $C_{nv} \otimes C_s$, and the additional symmetry element (horizontal mirror plane σ_h) does not affect the $E_\alpha \otimes e_\beta$ JT properties.
- ²⁶H. A. Jahn and E. Teller, *Proc. R. Soc. London, Ser. A* **161**, 220 (1937).
- ²⁷P. R. Wallace, *Phys. Rev.* **71**, 622 (1947).
- ²⁸Accurate and fully converged quantum dynamics simulations have been carried out using the discrete variable representation (DVR) approach to set up the 2D Hamiltonian, which then is diagonalized by an accurate short iterative Lanczos algorithm. Two sets of calculations have been performed one with a harmonic oscillator basis (Hermite DVR) and the other with a plane wave basis (Fourier transform DVR). The two different bases were used in order to analyze different aspects of the resulting wave functions more easily.
- ²⁹Note: The e_β coordinate is symmetric with respect to C_β rotation, and $\beta = 2$ is a divisor of $n = 6$ for the C_{6v} $E_\alpha \otimes e_2$ JT system. Thus, only $n/\beta = 3$ equivalent PES wells are obtained.